Experimental investigation of the variability of concrete durability properties

Abdelkarim Aît-Mokhtar, Jean Michel Torrenti, Farid Benboudjema, Bruno Capra, Myriam Carcasses, Jean-Baptiste Colliat, François Cussigh, Thomas de Larrard, Jf Lataste, Stéphane Poyet, et al.

Experimental investigation of the variability of concrete durability properties.

A. Aït-Mokhtar[a], R. Belarbi[a], F. Benboudjema[b], N. Burlion[c], B. Capra[d], M. Carcassès[e], J-B. Colliat[b], F. Cussigh[f], F. Deby[e], F. Jacquemot[g], T. de Larrard[b], J-F. Lataste[h], P. Le Bescop[i], M. Pierre[i], S. Poyet[i], P. Rougeau[g], T. Rougelot[c], A. Sellier[e], J. Séménadisse[f], J-M. Torrenti[j], A. Trabelsi[a], Ph. Turcry[a], H. Yanez-Godoy[d]

[a] Université de La Rochelle, LaSIE FRE-CNRS 3474, Avenue Michel Crépeau, F-17042 La Rochelle Cedex 1, France.
[b] LMT/ENS Cachan/CNRS UMR 8535/UPMC/PRES UniverSud Paris, 61 Avenue du Président Wilson, F-94235 Cachan, France.
[c] Laboratoire de Mécanique de Lille, Boulevard Paul Langevin, Cité Scientifique, F-59655 Villeneuve d'Ascq Cedex, France.
[d] Oxand, 49 Avenue Franklin Roosevelt, F-77210 Avon / Fontainebleau, France.
[e] Université de Toulouse, UPS, INSA, LMDC (Laboratoire Matériaux et Durabilité des Constructions), 135 Avenue de Rangueil, F-31077 Toulouse Cedex 4, France.
[f] Vinci Construction France, Direction des Ressources Techniques et du Développement Durable, 61 Avenue Jules Quentin, F-92730 Nanterre Cedex, France.
[g] CERIB, Rue des Longs Réages, BP 30059, F-28231 Epernon, France.
[h] Université Bordeaux 1, I2M CNRS UMR5295, Avenue des facultés, Bât. B18, F-33400 Talence, France.
[i] CEA, DEN, DPC, SECR, Laboratoire d'Etude du Comportement des Bétons et des Argiles, F-91191 Gif sur Yvette Cedex, France.
[j] Université Paris-Est, IFSTTAR, 58 Boulevard Lefebvre, F-75732 Paris Cedex 15, France.

Abstract

One of the main objectives of the APPLET project was to quantify the variability of concrete properties to allow for a probabilistic performance-based approach regarding the service lifetime prediction of concrete structures. The characterization of concrete variability was the subject of an experimental program which included a significant number of tests allowing the characterization of durability indicators or

performance tests. Two construction sites were selected from which concrete specimens were periodically taken and tested by the different project partners. The obtained results (mechanical behavior, chloride migration, accelerated carbonation, gas permeability, desorption isotherms, porosity) are discussed and a statistical analysis was performed to characterize these results through appropriate probability density functions.

Keywords: concrete – durability indicators – performance tests – variability.

1. Introduction / context

The prediction of the service lifetime of new as well as existing concrete structures is a global challenge. Mathematical models are needed to assess to allow for a reliable prediction of the behavior of these structures during their lifetime. The French APPLET project was undertaken in order to improve these models and improve their robustness [1]. The main objectives of this project were to quantify the various sources of variability (material and structure) and to take these into account in probabilistic approaches, to include and to understand in a better manner the corrosion process, in particular by studying its influence on the steel behavior, to integrate knowledge assets on the evolution of concrete and steel properties in order to include interface models between the two materials, and propose relevant numerical models, to have robust predictive models to model the long term behavior of degraded structural elements, and to integrate the data obtained from monitoring or inspection.

Within this project, working group 1 (WG1) has taken into consideration the variability of the material properties for a probabilistic performance-based approach of the service lifetime prediction of concrete structures. This determination of the variability of various on site

concretes was the subject of an experimental program with a significant number of tests allowing the characterization of indicators of durability or tests related to durability. After the presentation of the construction sites where the concrete specimens were produced in industrial conditions (using ready mix plants), the obtained results of the different tests (mechanical behavior, chloride migration, carbonation, permeability, desorption isotherms, porosity) are discussed and probability density functions are associated to these results.

2. Case studies

The objective of the project was the characterization of the variability of concretes produced in industrial conditions. This variability is due to the natural variability of the constituents of concrete, to errors in constituents weighing, to quality of vibration and compaction, to the initial concrete temperature, to environmental conditions, etc. For the supply of specimens, the project takes advantage from the support of Vinci Construction France. Two construction sites where two concretes were prepared continuously during at least 12 months regularly provided specimens to the various participants for the execution of their tests: works for the south tunnel in Highway A86 (construction site A1) and for a viaduct near Compiègne (north of Paris - construction site A2).

The first specimen denoted A1-1 was cast on 6th March 2007 at the tunnel construction site (Table 1), and then specimens were prepared and provided with a frequency of about one week. The concrete was a C50/60 (characteristic compressive strength at 28 days) containing Portland cement (CEM I) and fly-ashes used for the construction of the slab separating the two lanes from the tunnel of Highway A86 (Table 1). The concrete was prepared using the concrete plant on site by the site workers. Forty batches were made on this first construction site. The last specimen was cast on the 31st March 2008. In fact, for each date, 15 specimens (cylinders with a diameter of 113 mm and a height of 226 mm;

58 note that these shape and dimensions are accepted by the European standards EN 12390 and the French version of the ENV 206-1) were
59 produced and dispatched to the 7 laboratories participating in the project.

60 At the second construction site a concrete C40/50 was produced containing CEM III cement which was used for the construction of the
61 supports (foundations, piles) of the viaduct of Compiegne (Table 1). The first specimens (A2-1) were produced the 6th of November 2007 at the
62 viaduct construction site. The concrete was also prepared by the site workers using a ready mix concrete. However, from batch A2-21 on, due to
63 work constraints another composition corresponding to the same concrete quality was used to improve the concrete workability (denoted A2/2).
64 Finally, forty batches were produced, each composed of 14 specimens dispatched to the 7 laboratories involved. The last batch was produced the
65 21st of January 2009.

66

67 Table 1 - Concrete mixes (per m^3 of concrete).

Site	A1	A2/1	A2/2
Cement C	CEM I 52.5 - 350 kg	CEM III/A 52.5L LH - 355 kg	
Additions A	Fly ash - 80 kg		Calcareous filler - 50 kg
Water W	177 L	176 L	193 L
W/C	0.51	0.50	0.54

68

69 It must be added here that all the specimens used in this project were prepared on the two sites by the site workers simultaneously to the
70 fabrication of the slabs and supports of the construction sites A1 and A2, respectively. In the authors' mind, the concrete specimens are then
71 made of "realcrete" and are believed to be more or less representative of the materials that can be encountered within the considered
72 structures. Nonetheless it must be kept in mind that the variability obtained in this study might just be a rough estimate of the variability of the

corresponding structural elements because the impact of some worksite features (for instance presence of reinforcement, structural element dimensions and height of chute) could not be reproduced using small specimens.

3. Experimental results

3.1. Compressive and tensile strengths

This part of the research aims at proposing a characterization of the mechanical behavior of each studied batch by standard tests to determine the tensile strength (by a splitting test), and also the compressive strength and Young's modulus (through a compression test). The tests were performed at LMT of the Ecole Normale Supérieure de Cachan. For each batch, a cylindrical 113×226 mm specimen is devoted to compression test, while the splitting test is performed on a cylindrical specimen of 113 mm in diameter and 170 mm in height (the upper part of the specimen is used for porosity and pulse velocity measurements).

For the compression test, the specimen is mechanically grinded before being placed in press. The specimen is equipped with an extensometer (three LVDTs positioned at 120 degrees attached to a metal ring, which is fixed on the concrete specimen by set screws) to measure the longitudinal strain of the specimen during the loading phase assumed to be elastic, between 5 and 30% of the failure load in compression. Three cycles of loading and unloading are performed in the elastic behavior region of the concrete, with a loading rate of 5 kN/s (the rate is the same for unloading). Young’s modulus is determined by linear regression on five points placed on the curve corresponding to the third unloading, according to the protocol proposed by [2]. Then, after removing the extensometer, the specimen is loaded until failure.

89 Table 2 and Figure 1 to Figure 3 present an overview of the results derived from the mechanical tests (mean value, standard deviation,
90 coefficient of variation[1] and number of specimens tested). It can be observed that the compressive strength is much higher than expected
91 according to the compressive strength class and to the achieved values of compressive strength at 28 days (measured on site). This is due to the
92 fact that the specimens were tested after one year of curing in saturated lime water resulting in a higher hydration degree which improves the
93 strength. The magnitude of the coefficient of variation is similar for the compressive and tensile strengths: around 10%. However, the variability
94 observed for Young's modulus is significantly lower (between 5 and 7%).
95

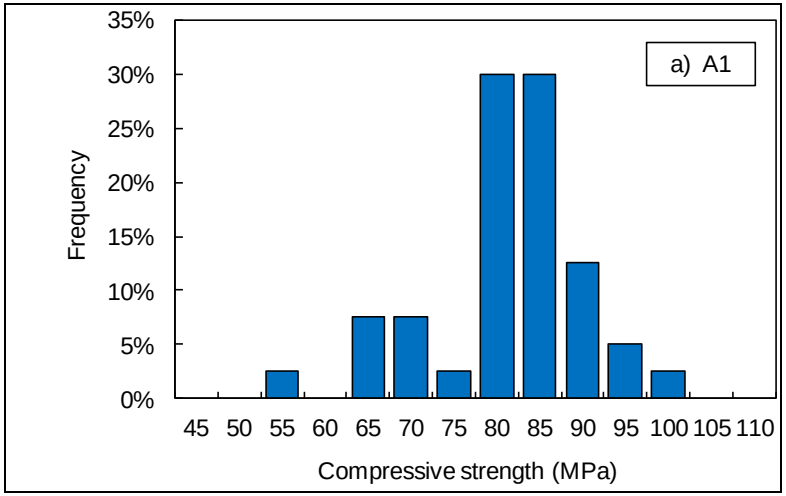

[1] The coefficient of variation (COV) is defined as the ratio of the standard deviation to the mean value. It is an indicator of the dataset dispersion.

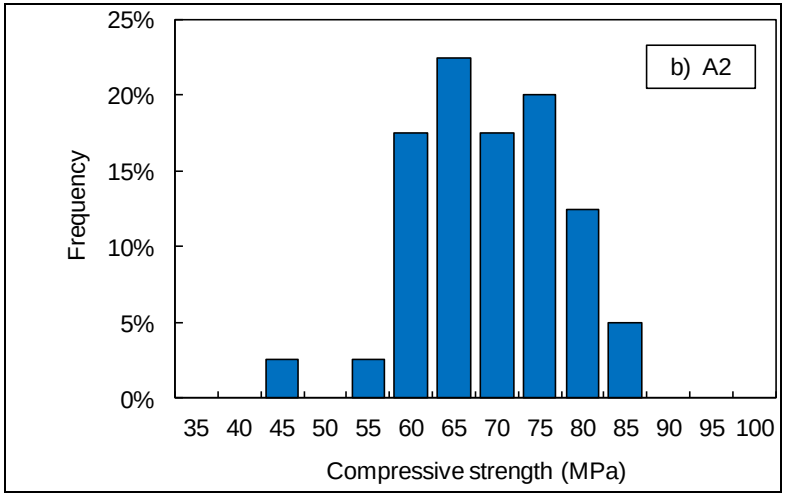

96 Figure 1 – Distribution of the compressive strength measured in laboratory (LMT) after 1 year curing.

97

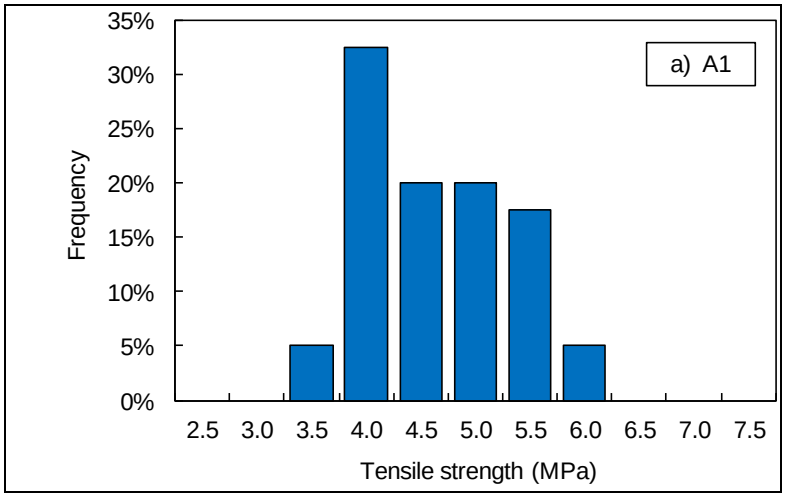

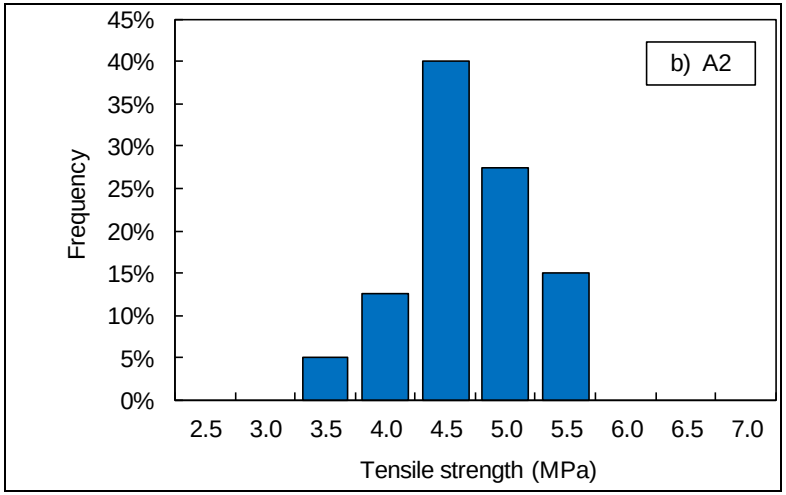

98 Figure 2 – Distribution of the tensile strength measured in laboratory (LMT) after 1 year curing.

99

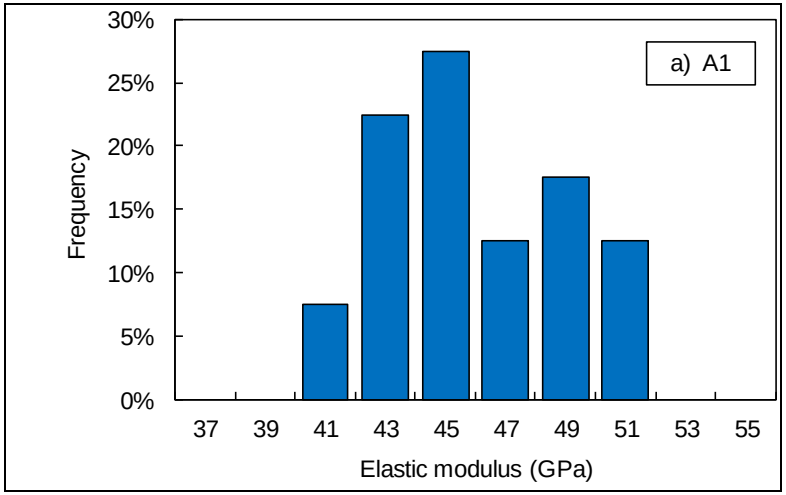

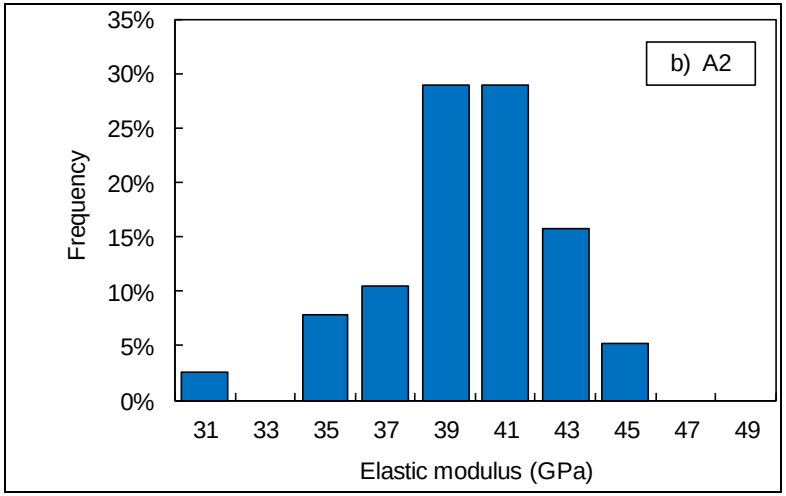

Figure 3 – Distribution of the elastic modulus measured in laboratory (LMT) after 1 year curing.

Table 2 - Mechanical tests for 3 concrete mix designs: mean values, coefficient of variation and number of specimens tested for the compressive (f_c) and tensile (f_t) strengths and Young's modulus (E).

Site	Number	f_c [MPa]		f_t [MPa]		E [GPa]	
		Mean	COV (%)	Mean	COV (%)	Mean	COV (%)
A1	40	83.8	10.5	4.9	13.2	46.8	6.2
A2-1	20	75.6	11.3	5.1	9.7	40.8	7.0
A2-2	20	68.2	9.0	4.8	9.3	40.8	5.4

The magnitude of the coefficient of variation is similar to what Mirza *et al.* [3] and Chmielewski & Konokpa [4] have observed for the variability of the compressive strength for "monitored" concrete (produced with great care), but their strengths were lower than those of the APPLET project materials. For high-performance concrete, having a compressive strength that is similar to that observed within this study, the variability observed by Torrenti [5] and Cussigh *et al.* [6] is approximately two times lower than it is here.

Simultaneously, the compressive strengths were also measured on site at age of 28 days. The specimens used were fabricated and kept in the same way as the ones that were sent to the involved laboratories. The tests were performed by Vinci Construction France using the same test conditions as detailed above. 116 specimens were tested for the construction site A1 and 114 for the construction site A2 (that is to say three different specimens from the same batch were tested at the same time except for some batches for which only two specimens were used). The results obtained for the variability are very similar to the previous ones (Table 3 and Figure 4).

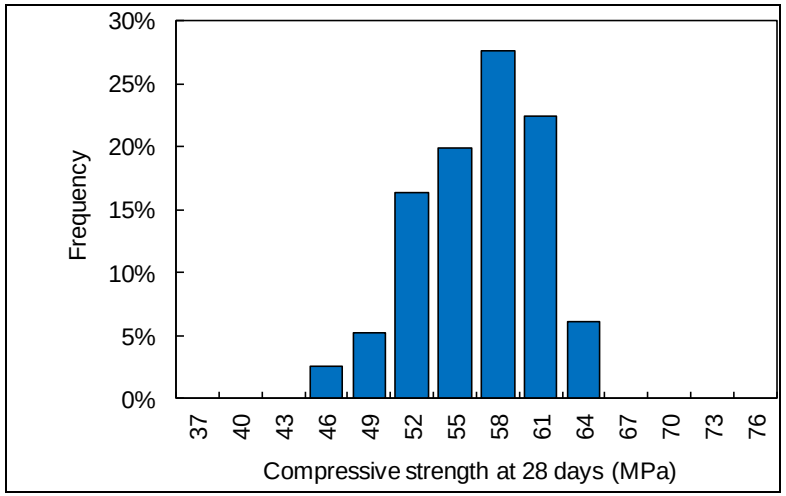

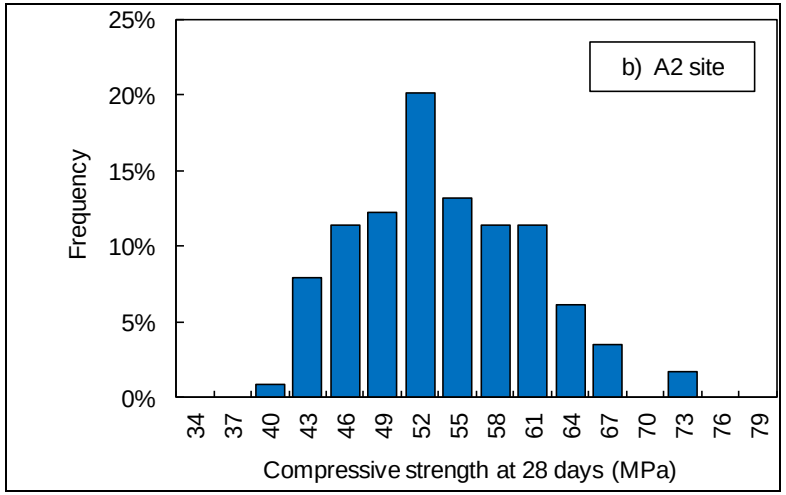

Figure 4 – Distribution of the compressive strength (at 28 days) measured on site by Vinci Construction France.

Table 3 – Compressive strength measured on site by Vinci Construction France: number of tests (Nb), mean value and coefficient of variation (COV).

Site	Nb	f_c [MPa]	
		Mean	COV (%)
A1	40	58.2	7.3%
A2-1	20	57.8	11.1%
A2-2	20	52.6	11.1%

3.2. Chloride migration

Non-steady state migration tests have been performed at LMDC (Toulouse University) in order to measure the chloride migration coefficient. For the two selected construction sites, an overview of the results will be presented in the following sections.

The principle of the test method is described in the standard NT Build 492 [7]. The specimens were kept in water until the start of the test. The experiments were performed for similar maturity of each specimen in the same series in order not to introduce on the results the effect of

125 the evolution of the concrete. Due to the equipments and the constraints of organizing this extensive significant experimental campaign,
126 experiments were launched at an age of 3 months for the A1 series and an age of 12 months for A2. Furthermore, it should be noted that logistic
127 problems were encountered: some deadlines were not respected and in these situations, the test was not conducted. Consequently, on the 40
128 initially planned, only 30 specimens from the A1 series and 31 from the A2 series were tested.

129 At the date of test, the specimen is then prepared. Once out of the storage room, specimens are cut to retain only a cylinder Ø113mm of
130 50mm height. The test specimen is taken from the central part of the specimen by cutting the top 50 millimeters from the free surface. The
131 concrete surface closest to the latter is then exposed to chlorides (Figure 5).

132

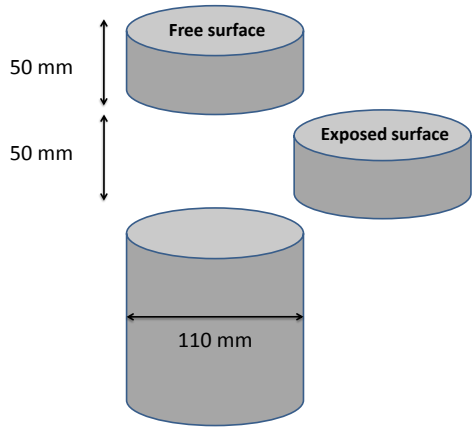

133
134 Figure 5 – Specimen preparation for the chloride migration test.

135

136 The specimen is then introduced in a rubber sleeve, and after clamping, sealing is ensured by a silicone sealant line. At first a leakage test is
137 performed to detect any failure. The extending part of the sleeve is used as downstream compartment while the cell migration (a plastic box

which receives the sleeve) corresponds to the upstream compartment. The upper compartment contains the catholyte solution, i.e. a solution of 10% sodium chloride by mass (about 110 grams per liter) whereas the downstream compartment is filled with the anolyte solution, 0.3 M sodium hydroxide. These solutions are stored in the conditioned test room at 20 °C. In each compartment an electrode is immersed, which is externally connected through a voltage source so that the cathode, immersed in the chloride solution, is connected to the negative pole and the anode, placed in the extending part of the sleeve, is connected to the positive pole. An initial voltage of 30 V is applied to the specimen. This voltage is then adjusted to achieve a duration test of 24 hours depending on the magnitude of the current flowing through the cell as a result of the initial voltage of 30 V. The correction is proposed in the standard NT Build 492 [7]. For A1 specimens, for the entire series the voltage used for the test is 35 V whereas 50 V is applied for the entire A2 series.

After 24 hours, the specimen is removed to be split in two pieces. Silver nitrate $AgNO_3$ is then sprayed onto the freshly fractured concrete surface. The white precipitate of silver chloride appears after ten minutes revealing the achieved chloride penetration front. At the concrete surface where chlorides are not present silver nitrate will not precipitate but will quickly oxidize and then turn black after a few hours. The chloride penetration depth in concrete x_d is then measured using a slide caliper using an interval of 10 mm to obtain 7 measured depths. To avoid edge effects, a distance of 10 mm is discarded at each edge. Moreover, if the front ahead of a measuring point is obviously blocked by an aggregate particle, then the associated measured depth is rejected. Then the migration coefficient D_{nssm} (non steady state migration) (m^2/s) is calculated using the following formula:

$$D_{nssm} = \frac{0.0239(273+T)\cdot L}{(U-2)t}\left(x_d - 0.0238\sqrt{\frac{(273+T)Lx_d}{U-2}}\right) \quad (1)$$

155

156 where U is the magnitude of the applied voltage (V), T the temperature in the anolyte solution (°C), L the thickness of the specimen (mm), x_d the
157 average value of the chloride penetration depth (mm) and t the test duration (h). All the results are shown in Figure 6 which shows the migration
158 coefficient obtained for the specimens from the A1 series.

159 The measured values vary around a mean value of 4.12×10^{-12} m²/s. The potential resistance against chloride ingress is then high. This can be
160 easily explained by the formulation of this C50/60 concrete where fly ash was used, which is known to significantly reduce the diffusion
161 coefficient [8]. The minimum value observed is 3.11×10^{-12} m²/s and the maximum amounts to 5.59×10^{-12} m²/s which corresponds to a ratio of
162 1.8. The difference may seem relevant but basically corresponds to a divergence in concrete porosity of about 1.5% if the migration coefficients
163 are estimated from basic models [9]. The standard deviation is equal 0.53×10^{-12} m²/s; this corresponds to a coefficient of variation of 12.4%
164 (Table 4).

165

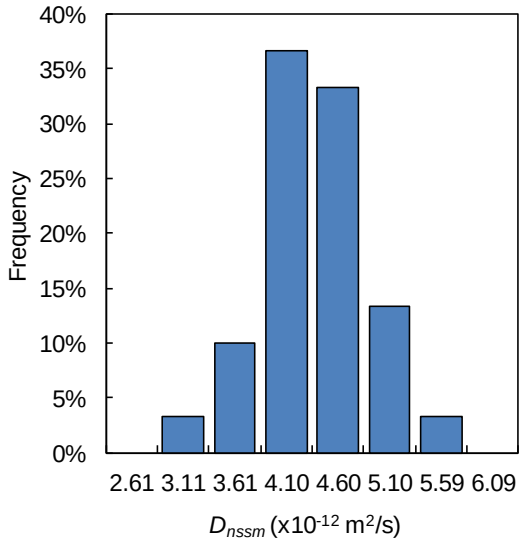

Figure 6 – Histogram of the migration coefficient from the A1 series.

For the A2 series the experiments could not be conducted on specimens A2-12 to A2-20. The migration experiments have been resumed from A2-21, which corresponds to the modified mix design of the A2 series. The mean migration coefficients determined for the complete A2 series is 2.53×10^{-12} m²/s with a standard deviation of 0.55×10^{-12} m^2/s corresponding to a coefficient of variation of 21.9%. Compared to the concrete of the A1 series, the resistance of this concrete against chloride ingress is significantly higher. The average value is even smaller however for this A2 series concrete specimens were tested at a later age, i.e. one year instead of three months for A1. The second concrete (A2) would certainly achieve more modest results at a younger age because of the slow hydration kinetics for this type of cement containing blast furnace slag.

In the same way as for the A1 series, all these results may be grouped in a histogram. In contrast, as A2 series contains two mix design formulations, the results must be treated in two subsets. In addition, the first formulation contains only 11 results, whereas the histogram of the

second formulation of this A2 reflects 20 experimental values (Figure 7). The mean migration coefficient of the second formulation of the A2 series amounts to 2.45×10^{-12} m²/s with a standard deviation of 0.47×10^{-12} m²/s, which corresponds to a coefficient of variation of 19.4% (Table 4). It should be noted that the mean value and coefficient of variation are lower for the second formulation of the A2 series. This corresponds to observations on site (higher variability of the workability for A2-1) that has decided the Vinci Company to modify the formulation.

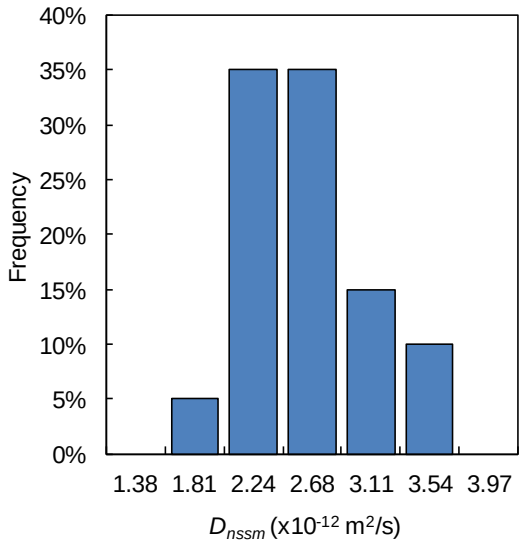

Figure 7 – Histogram of the migration coefficient for the A2-2 series.

The variability is higher than for the A1 series since the coefficient of variation increases from 12.4% to 19.5% (and even larger if A2-1 consider is considered).

Table 4 – Migration coefficient: number of tests (Nb), mean value and coefficient of variation (COV).

Site	Nb	D_{nssm} [10^{-12} m^2/s]	
		Mean	COV (%)
A1	30	2.53	12.4%
A2-1	11	2.67	25.4%
A2-2	20	2.45	19.4%

3.3. Water Vapour desorption isotherm

Water vapour sorption-desorption isotherms tests were performed at the LaSIE at La Rochelle University [10]. This test characterizes water content in a porous medium as a function of relative humidity at equilibrium state. It expresses the relationship between the water content of the material and relative humidity (RH) of the surrounding air for different moisture conditions defined by a RH ranging from 0 to 100%.

The method undertaken in this study for the assessment of desorption isotherms is based on gravimetric measurements [11, 12]. Specimens were placed in containers under isothermal condition (23 ± 1°C). The relative humidity of the ambient air is regulated using saturated salt solutions. For each of the following moisture stages: RH = 90.4%, 75.5%, 53.5%, 33%, 12% and 3%, a regular monitoring of mass specimen in time was performed until equilibrium was obtained characterized by a negligible variation of relative mass. The weighing of specimens was performed inside the container as to result into the least disturbance of the relative humidity during measurements. The equilibrium is assumed to be achieved if the hereafter criterion is satisfied:

$$\frac{m(t)-m(t+24h)}{m(t+24h)} \leq 0.005\% \qquad (2)$$

where $m(t)$ is the mass measured at the moment t and $m(t + 24h)$ is the measured mass 24 hours later.

The test started with specimens which were initially saturated. To achieve the saturation, the adopted procedure consists in storing the cylindrical specimens Ø113×226mm under water one day after mixing during at least 4 months. Besides, this procedure promotes a high degree of hydration of cement. At the age of 3 months, these specimens were sawn in discs of 113 mm diameter and 5 ± 0.5 mm thickness. In these discs a 4 mm diameter hole was drilled allowing mass measurements to be made inside the controlled RH environment with an accuracy of 0.001 g. At construction site A1, 3 specimens 113×226mm per batch were used and in the case of construction site A2, only the first concrete composition (*i.e*. A2-1) was studied with 3 specimens per batch and overall, 180 specimens were studied.

Figure 8 shows the isothermal desorption curves for compositions A1 and A2-1. The water contents at equilibrium for the different RH levels were calculated on the basis of dry mass measured at the equilibrium state for 3% RH. The so-obtained desorption isotherms belong to type IV according to the IUPAC classification [13]. These are characterized by two inflections which are often observed for such a material [12]. Desorption is thus multi-molecular with capillary condensation over a broad interval, which highlights a pore size distribution with several modes (i.e. with several inflections points. For a given RH, concrete mixture A2-1 has higher average water content, especially for RH levels above 50%. This is rather consistent with the mix proportions since mixture A2-1 has higher initial water content than mixture A1.

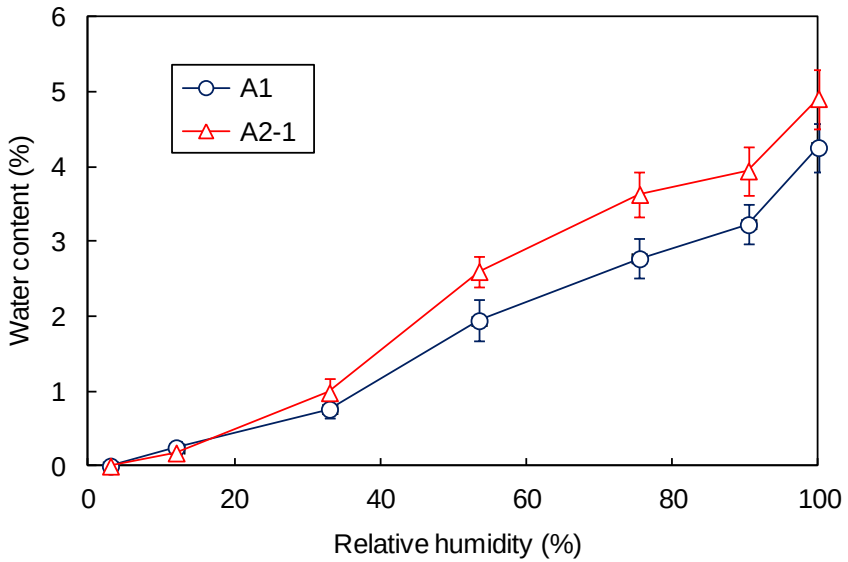

Figure 8 – Average isothermal desorption curves for mixtures A1 and A2-1.

Table 5 gives the average water content values calculated at equilibrium with the different tested humidity environments and the corresponding standard deviations and coefficients of variation. The coefficient of variation for 3 specimens from a single batch is approximately equal to 10% for RH levels between 100 and 33% and equal to 20% for RH = 12%. The coefficients of variation determined over the complete construction period (given in Table 5) are higher than the coefficients of variation for a single batch. The observed dispersion is not only due to the randomness of test measurements, but also due to variability of material properties under site conditions [14]. It should be recalled that mixtures were made in real ready-mix concrete plants.

Table 5 – Water vapour desorption isotherm: average values, standard deviations (Std dev.) and coefficients of variations (COV) of water contents at equilibrium (throughout the construction period).

Concrete	RH	12%	33%	53.5%	75.5%	90.4%	100%
A1	Mean (%)	0.2	0.8	1.9	2.8	3.2	4.3
	Std dev. (%)	0.09	0.13	0.27	0.27	0.26	0.33
	COV (%)	45	16	14	10	8	8
A2-1	Mean (%)	0.2	1.0	2.6	3.6	3.9	4.9
	Std dev. (%)	0.08	0.17	0.18	0.31	0.35	0.39
	COV (%)	40	17	7	9	9	8

As shown in Figure 9, the statistical distributions of the water contents at equilibrium can be adequately modeled by normal probability density functions. The parameter values of the normal probability density functions determined through regression analysis are given in Table 5.

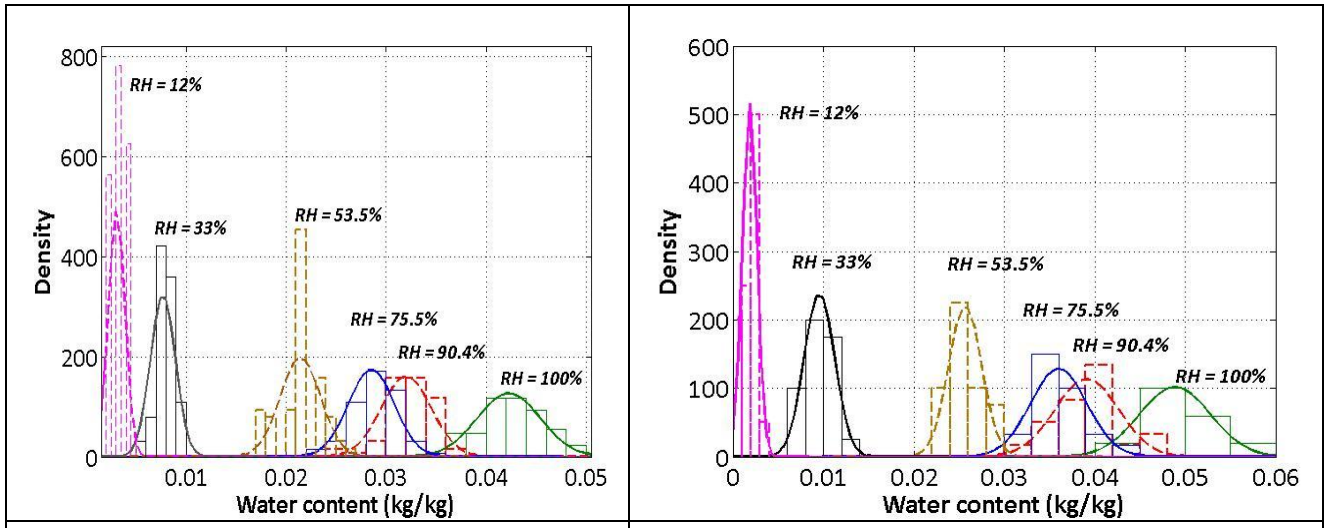

Figure 9 – Statistical distribution of water contents at equilibrium for A1 (a) and A2-1 concretes.

3.4. Carbonation

The carbonation tests were performed at the CERIB and at the LaSIE (University of La Rochelle). For more details, the reader is referred to [15]. From each construction site (A1 and A2), cylindrical specimens, 113mm in diameter and 226mm in height were sampled from different batches. On site A1, 1 specimen per batch was sampled from the last 10 batches. On site A2, 3 specimens per batch were taken from 40 subsequent batches. After water curing during at least 28 days, each specimen was sawn at mid-height in order to obtain a disc, 113mm in diameter and 50mm in height.

The protocol of the accelerated carbonation test is described in the French Standard XP P18-458. Concrete discs were first oven-dried at 45 ± 5°C during 14 days. After this treatment, the lateral side of the disks was covered by adhesive aluminum in order to ensure an axial CO_2 diffusion during the carbonation test. The discs were then placed in a chamber containing 50 ± 5% CO_2 at 20 ± 2°C and 65% RH. After 28 days in this environment, the concrete discs were split into two parts. A pH indicator solution, i.e. phenolphthalein, was sprayed on the obtained cross sections in order to determine carbonation depth. The reported carbonation depth is the mean value of 24 measured depths per disc.

Table 6 gives an overview of the results of the accelerated carbonation tests. The average carbonation depth of A1 concrete is less than that of A2 concretes. This can be attributed to the difference in binder type used in the concrete mixtures: slag substitution is known to enhance carbonation [16, 17]. A significant difference can also be observed between the two mixtures from construction site A2. This difference might be explained by a higher connectivity of the porous structure induced by the air-entraining effect of the plasticizer used for the second mixture A2-2.

The variability of the results is rather high. Figure 10 shows the statistical distribution of the carbonation depth in the case of construction site A2. The distribution can be reasonably described by a normal probability density function (cf. §4.2).

Table 6 – Mean value, standard deviation and coefficient of variation of the carbonated depth.

Carbonation depth	A1	A2-1	A2-2	A2
Mean value (mm)	4.3	7.6	12.6	10.1
Standard deviation (mm)	1.6	2.6	1.5	3.3
COV	37%	35%	12%	33%

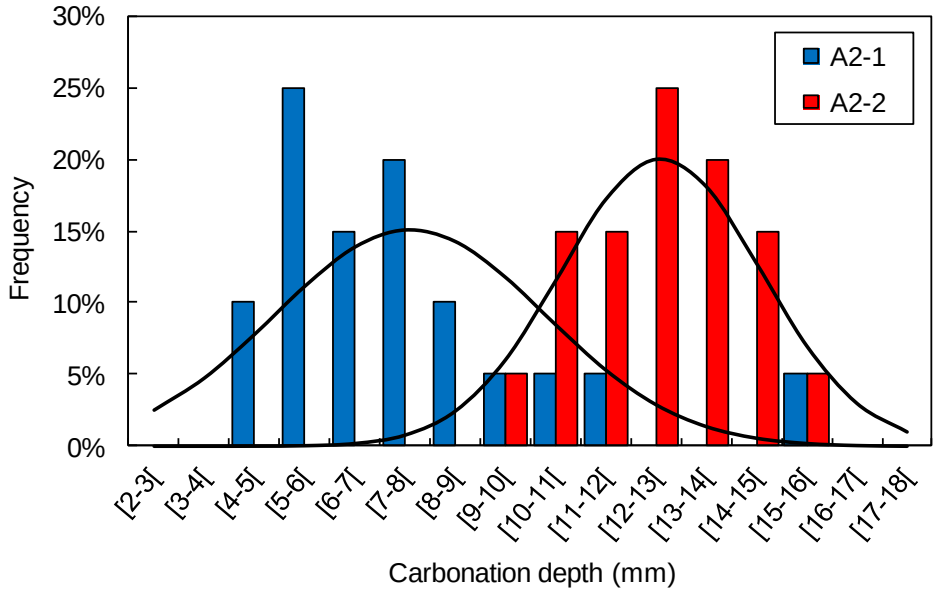

Figure 10 - Statistical distribution of the accelerated carbonation depths throughout the complete construction period (site A2).

3.5. Electrical resistivity

The electrical resistivity of concrete is generally a parameter measured on concrete structures to assess the probability of reinforcement corrosion. However, because of its dependence on the porosity of the material [18], developments have been made for the assessment of concrete transfer properties [19-21]. It appears increasingly as a durability indicator [18, 22].

The investigations done within the APPLET program, aim at assessing the reliability of resistivity measurements for concretes properties, by performing tests on 113×226mm cylindrical specimens using the resistivity cell technique in the laboratory. It consists in introducing an electrical current of known magnitude in a concrete specimen and measuring the potential difference thus generated between two sensors on the opposite specimen faces. Preliminary investigations have been done to study the influence of conditioning parameters on electrical resistivity measurements. Finally, a light process has been defined to store specimens before resistivity measurement in the laboratory [23].

The measurements have been performed at I2M in University Bordeaux1 (specimens having an age of 3 months, after continuous submersion in water) and at LMT (specimens of 1 year , after continuous submersion in a saturated lime solution), according to a protocol defined to distinguish different levels of variability [23]. The repeatability and reproducibility of laboratory measurement have been evaluated for each specimen; the variability of the material within a batch (2 batches consisting of 20 specimens each are studied), and the variability of the material during a year of casting (2 formulations studied from 40 specimens of test) are determined.

It is observed (Figure 11) that concrete A1 presents different ranges according to the laboratory: between 111 and 236 Ωm for 90 days old concrete, and between 282 and 431 Ωm for 1 year-old concrete. This difference can essentially be attributed to the ageing, as was already observed on concretes containing fly ash [24].

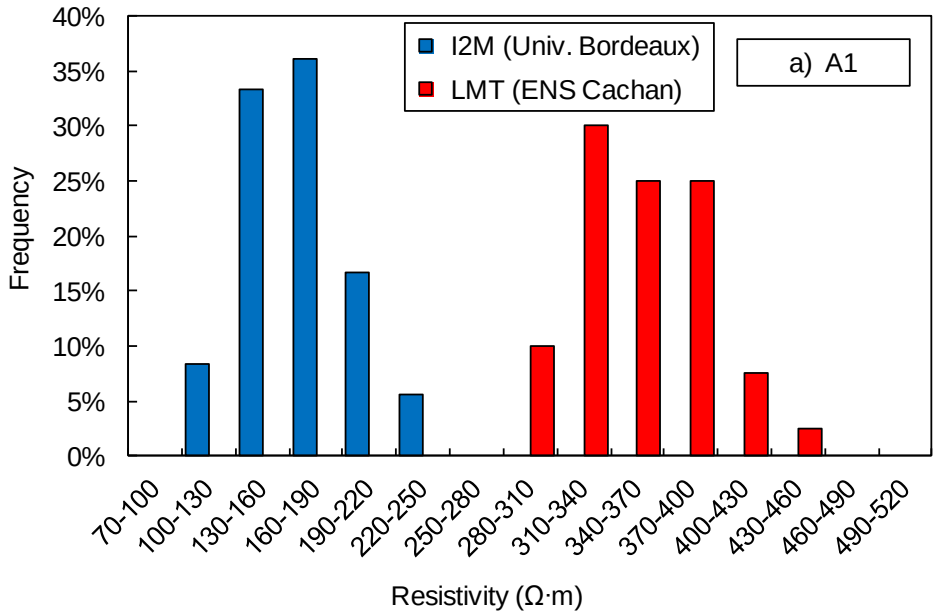

Figure 11 – Resistivity distribution for concrete A1 (the specimens used at I2M were 90 days old whereas the age was 1 year at LMT).

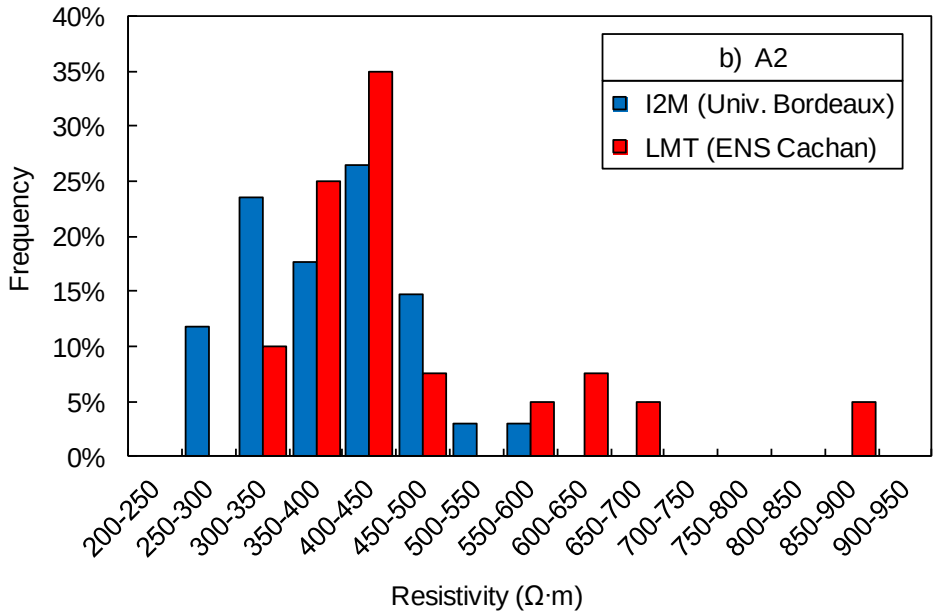

Figure 12 – Resistivity distribution for concrete A2 (the specimens used at I2M were 90 days old whereas the age was 1 year at LMT).

Concrete A2 (Figure 12) does not present this difference despite the age difference and although the cement contains a significant amount of slag. It is noted that both databases express a similar behavior even if measurements on 1 year old concrete show an expected light increase in resistivity. However, for the distribution tail (towards the high resistivity values) the measured values range from 266 to 570 Ωm at an age of 90 days, and from 324 to 898 Ωm at an age of 1 year. These results show the difficulty to compare concretes using their resistivity values. Electrical resistivity is a parameter which is very much influenced by the conditions during measurements (saturation degree of the specimen, temperature, the nature of the saturation fluid). An overview of the variability assessment for both concretes is given in Table 7.

Table 7 – Electrical resistivity (Ωm): variability observed in laboratory.

Organism/Laboratory		I2M	LMT	I2M	LMT
Concrete		A1	A1	A2	A2
Device used		Resistivity cell	Resistivity cell	Resistivity cell	Resistivity cell
Mean value		166.8	352.5	391.2	461.7
Mean repeatability	r	0.005	-	0.007	-
Mean reproducibility	R	0.015	0.006	0.012	0.007
Variability within a batch *	Vb	0.023	0.076	0.036	0.035
Variability between batches	VB	0.176	0.114	0.182	0.296
Age at measurements		90 days	1 year	90 days	1 year
		* 590 days	* at each term	* 436 days	* at each term

Variability linked to measurements is the repeatability (which characterizes the equipment), and the reproducibility (which also estimates the noise due to the protocol). Whatever the concrete and laboratory are, it is concluded that these variabilities are good. They are indeed less than 2 % and underline that in laboratory the measurement results are accurate. The variability within a batch (Vb) is generally less than 5 % (except for one year old concrete A1 which remains however less than 8 %). The variability between batches (VB) is determined to be less than 20 % (except for the one year old concrete A2 which reaches 29.6 %, but this can be explained by the modification of the mix design during the construction period).

Whatever the laboratory or the set of specimens considered, the variability is always ranked consistently: r <R <Vb <VB. The values of r and R being low, variability Vb and VB are therefore only representative of the material variability. So, it is surprising to observe relatively large range, for materials the engineer considers to be homogeneous and identical. These measurements show: (1) within a batch there are significant differences between specimens; (2) for a single concrete cast regularly during one year, variability is less than 20%.

The differences observed between laboratories emphasize the importance of measurement conditions. Only measurements performed under controlled conditions, regardless of the type of the specimen, should be considered. Any change in the conditioning (for instance temperature, saturation or age) influences the resistivity values measured.

Resistivity measurements have also been done on a wall on site, made of A1 concrete, at an age of 28 days. On site value of reproducibility is slightly higher than for the laboratory measurements (4.8%).

These results illustrate that the conditions of on-site measurements are less controlled. Even though this study is not sufficient to link the variability of the concrete specimens to the concrete structural elements, it is however observed that on-site measurement and laboratory techniques are consistent [23].

3.6. Porosity

3.6.1 Experimental setup

For the A1 construction site, specimens are denoted A1-x where x is the batch number (from 1 to 40). For the A2 construction site, as 2 different concrete mixes were studied (20 weeks for the first mix, then 20 weeks for the second), the specimens are denoted A2-y-x, where y is the mix number (1 or 2) and x the batch number (specimen numbers range from A2-1-1 to A2-1-20, then A2-2-21 to A2-2-40). The determination of porosity is studied through cylindrical specimens (diameter: 113 mm – height: about 50 mm) sawn from the bottom part of the bigger cylindrical moulded specimens. This study was performed at the LMT. In particular, these tests aimed at analyzing the variability with respect to the batch number (one batch per week); that is to say the ‘temporal variability’ of a given concrete.

319 Secondly, the variability of porosity inside a given concrete batch is also studied. Additional cylindrical moulded specimens of batch A1-13 and
320 A2-1-1 are cast. The porosity is determined on small cylindrical specimens (diameter: 37 mm – height: about 74 mm) cored from those cylindrical
321 moulded specimens. A total of 39 specimens are cored from batch A1-13, and 6 from batch A2-1-1. This study was performed in the LML (Lille 1
322 University).

323 Such small diameter (37 mm) or small height (50 mm) was chosen to limit the duration of the drying process and the needed time for the
324 experimentation. The specimens, until testing, were always kept immersed in lime saturated water at 20 ± 2°C for at least 6 months (12 months
325 for specimens used for temporal variability) to ensure a sufficient maturity and a very limited evolution of the microstructure. These storage
326 conditions tend also to saturate the porous network of the material.

327 In order to achieve a full water saturation state, AFPC-AFREM protocol [25] recommends maintaining an underpressure of 25 millibars for 4
328 hours and then to place the specimens under water (with the same underpressure) for 20 hours. Tests conducted at LMT highlight that for such
329 specimens kept under water during a long period, the effect of low underpressure (25 millibars) on water saturation will be negligible on water
330 saturation. Therefore, specimens used by LMT were only saturated during the immersion in lime-saturated water.

331 The same conclusions were drawn at LML. The additional saturation protocol is adapted from recommendations of AFPC-AFREM [25], mainly
332 by increasing the saturation time with underpressure. Specimens were placed in a hermetically closed box with a slight underpressure of 300
333 millibars and achievement of the saturation is assumed to be achieved when the mass variation is less than 0.1% per week. In both cases, the
334 mass change due to this saturation under vacuum is negligible (mass change in 3 weeks amounts to only 0.15%), and considering specimens to be
335 completely water saturated after at least 6 months of continuous immersion appears to be valid. This mass at saturation is noted m_{sat}. Then, the
336 volume of the specimens is determined through a hydrostatic weighing (mass m_{hydro}).

Finally, specimens are stored in an oven until mass equilibrium (change in mass less than 0.1% per week). The specimens used for the so-called 'temporal variability' are dried in an oven at 105°C until mass equilibrium as recommended in the AFPC-AFREM protocol [25]. The protocol is adapted for LML tests. The drying is conducted at 60°C until equilibrium, then the temperature is increased to 90°C and then to 105°C to study the effect of the drying temperature on experimental variability. The mass at a dried state (at a temperature T) is noted $m_{oven\text{-}T}$. The porosity at the temperature T is called $\phi(T)$ and can be determined as follows (equation 3).

$$\phi(T) = \frac{m_{sat} - m_{oven-T}}{m_{sat} - m_{hydro}} \quad (3)$$

3.6.2 Results

Figure 13 presents the distribution of porosity for the 40 specimens (directly dried at 105°C) received from the A1 construction site, from batch 1 to 40. This allows studying 'temporal variability' of the same concrete mix for several batches. In the same way, Figure 14 shows the distribution of porosity for the A2-1 mix (batch 1 to 20) and Figure 15 for the A2-2 mix (batch 21 to 40), measured by direct drying at 105°C. The average porosity, standard deviation and coefficient of variation are recapitulated in Table 8.

The porosity of A1 concrete is lower than for A2 concretes, as the composition and designed strengths are clearly different. The coefficient of variation for A1 and A2-1 mixes appears to be two times higher than for A2-2 (7.92% and 9% versus 3.96%). This could be partly explained by the low sensitivity of the A2-2 concrete to the small changes in composition (due to the gap between theoretical and real formulation).

353 Secondly, the study aims at quantifying more precisely the variability inside one particular batch (batches A1-13 and A2-1-1). Figure 16
354 presents the distribution of porosity on the 39 specimens from the batch A1-13 dried at 60°C (Figure 16a), then 90°C (Figure 16b) and finally
355 105°C (Figure 16c) from the batch A1-13. The values of average porosity, standard deviation, coefficient of variation and minimum and maximum
356 values are summed up in Table 9. The effect of temperature on porosity is clearly seen with an increase of the measured porosity from 10.1% to
357 11.5% between 60 and 105°C, but the statistical dispersion remains identical for the 3 tested temperatures. The role of drying temperature on
358 statistical dispersion is, as a consequence, negligible. Table 10 is the analogue of Table 9 but now for the 6 specimens from the A2-1-1 batch. The
359 same tendency is confirmed for specimens from the A2-1-1 batch, even if variability is lower (3.5% versus 6.44% at 60°C). This could be attributed
360 to a lower material variability.
361 Eventually, a last comparison between the protocol of LMT (direct drying at 105°C) and LML (stepwise drying at 105°C) can be made regarding
362 the porosity of A1-13 batch. It appears that the measured porosity is not the same (12.4% by LMT on 1 specimen, average of 11.5% by LML on 39
363 specimens). However, as the values of porosity on the 39 specimens range from 9.7 to 13.6%, it cannot be concluded that porosity is actually
364 different. Moreover, additional tests have been performed at the LML to check the effect on porosity of stepwise or direct drying at 105°C.
365 Porosity is always higher when specimens are immediately dried at 105°C rather than in steps at 60, 90 and then 105°C (porosity of 12.2% by
366 direct drying at 105°C versus 11.5%) [26]. As a consequence, it seems that the two protocols used by the LML or LMT can provide a reliable
367 characterization of porosity and its variability, provided that the drying method is clearly mentioned.
368

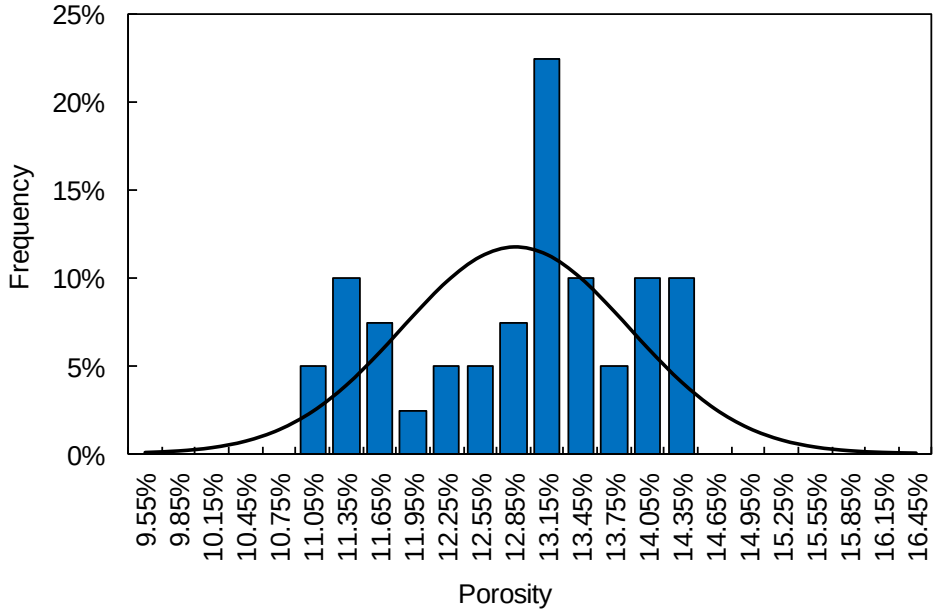

Figure 13 – Porosity distribution of A1 specimens (from batch 1 to 40) immediately dried at 105°C. The line is the fitted normal probability density function. Note that in this case, the normal probability density function does not fit well the results.

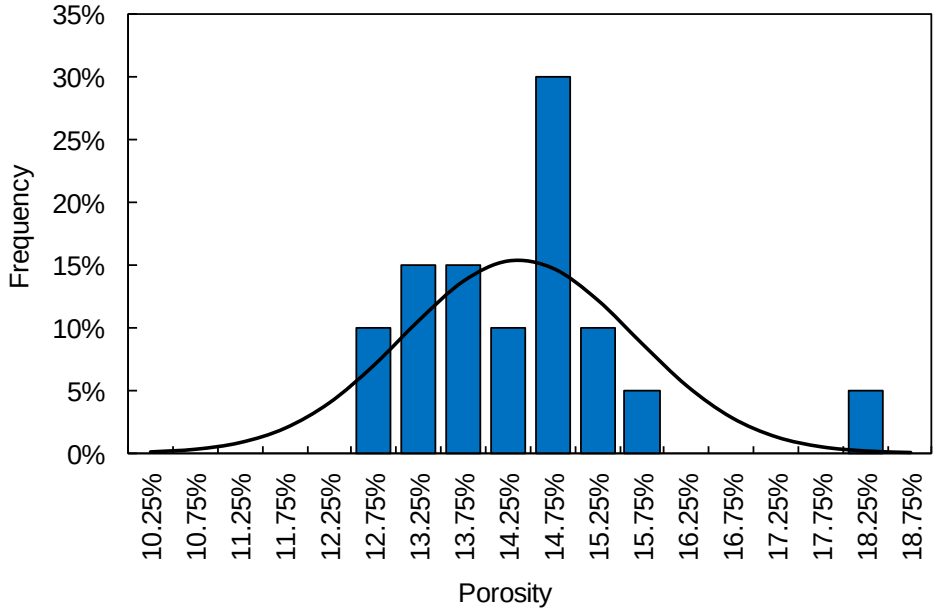

Figure 14 – Porosity distribution of A2-1 specimens (from batch 1 to 20) immediately dried at 105°C. The line is the fitted normal probability density function.

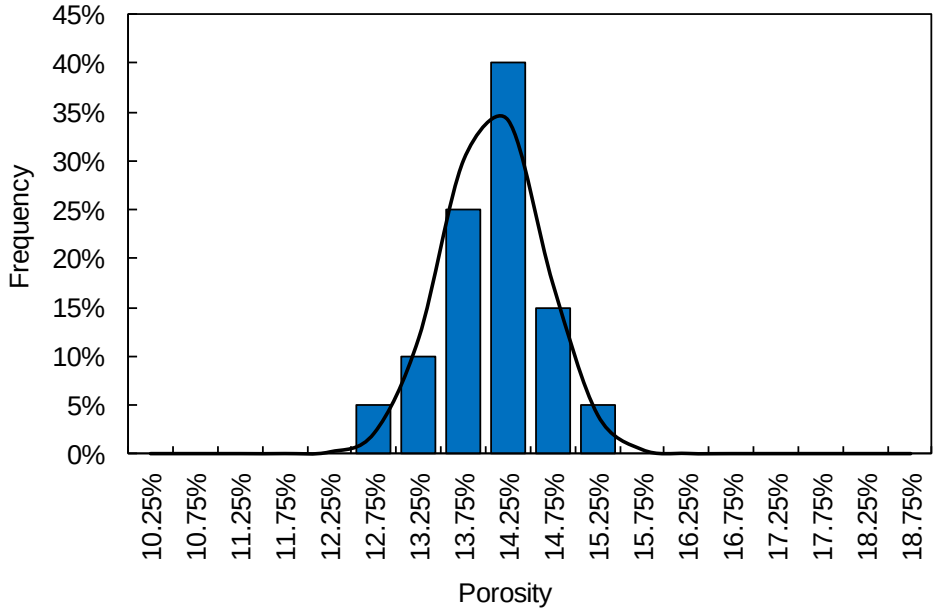

Figure 15 – Porosity distribution of A2-2 specimens (from batch 21 to 40) immediately dried at 105°C. The line is the fitted normal probability density function.

Table 8 – Statistical data on porosity versus concrete mix.

Concrete mix	A1	A2-1	A2-2
Average	12.9%	14.4%	14.1%
Standard deviation	1.02%	1.29%	0.56%
Coefficient of variation	7.92%	9.00%	3.96%
Minimum	11.1%	12.7%	12.9%
Maximum	14.4%	18.2%	15%

Table 9 – Statistical data on porosity versus drying temperature (39 specimens of batch A1-13).

Drying temperature	60°C	90°C	105°C
Average	10.1%	10.9%	11.5%
Standard deviation	0.65%	0.69%	0.75%

Coefficient of variation	6.44%	6.35%	6.49%
Minimum	8.5%	9.2%	9.7%
Maximum	11.8%	12.8%	13.6%

383

384 Table 10 – Statistical data on porosity versus drying temperature (6 specimens of batch A2-1).

Drying temperature	60°C	90°C	105°C
Average	12.1%	12.9%	13.4%
Standard deviation	0.43%	0.46%	0.47%
Coefficient of variation	3.50%	3.57%	3.54%

385
386
387

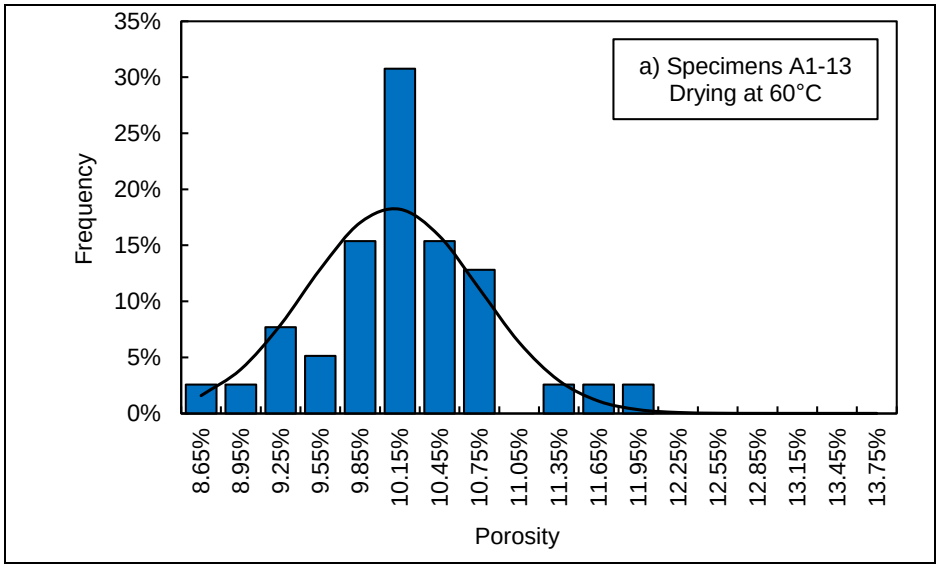

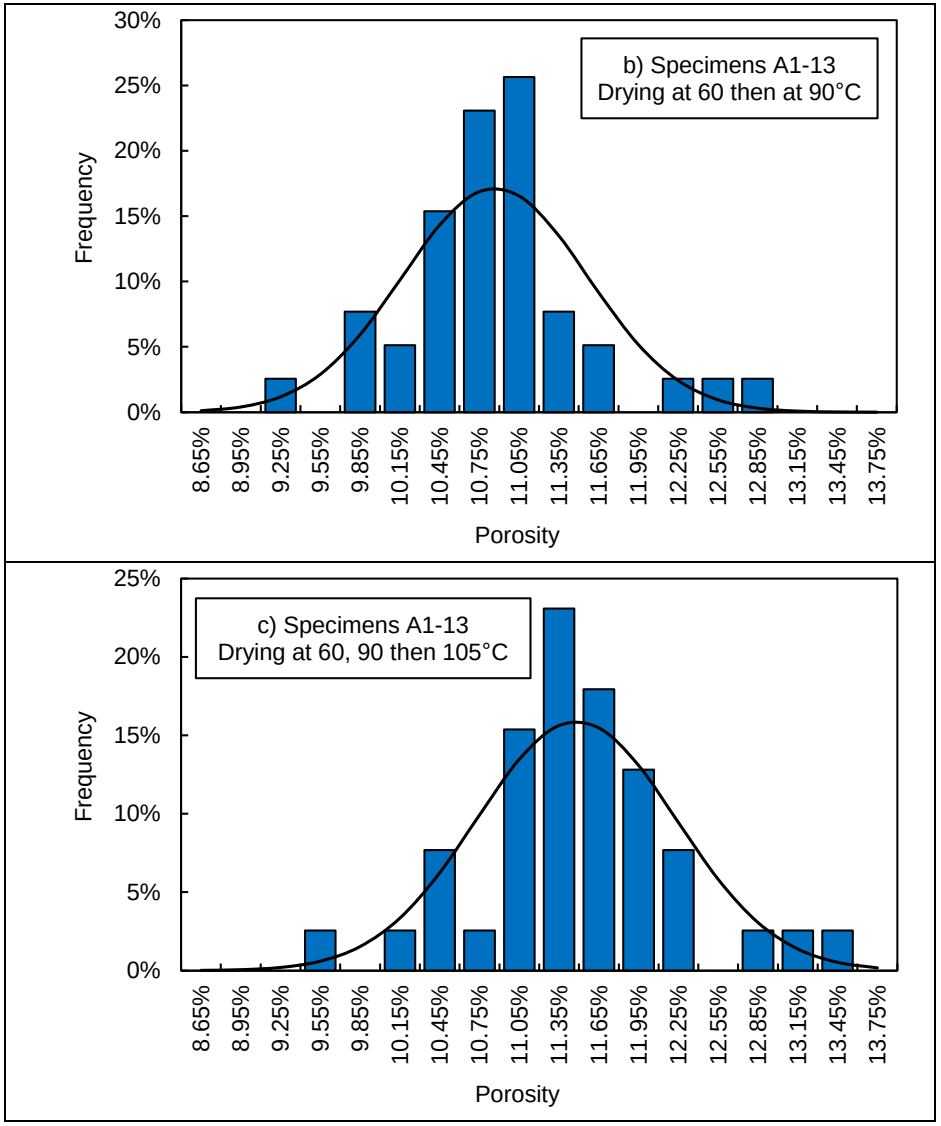

388 Figure 16 – Porosity distribution of A1-13 dried at: (a) 60°C, (b) then 90°C and (c) ultimately 105°C. The line is the fitted normal probability
389 density function.

390

3.7. Leaching

The characterization of concrete variability in relation to leaching was performed at LMT and will be described in the following section. Other complementary experiments were also conducted simultaneously at CEA to check the influence of temperature and tests conditions. These tests are not described in this article. For more details, the reader is referred to [27, 28].

The measurements performed in LMT within the APPLET project are accelerated tests using ammonium nitrate solution [29]. After a storage of about one year in lime saturated water, the specimens are immersed in a 6 mol/L concentrated NH_4NO_3 solution. The specimens are immersed in the ammonium nitrate solution 8 by 8, every 8 weeks. For security reasons, the containers with the aggressive solution and the specimens are kept outside the laboratory, and thus subjected to temperature variations. Therefore, a pH and temperature probe is placed in the container, so as to register once an hour the pH and temperature values in the ammonium nitrate solution. If the pH of the solution reaches the threshold value of 8.8, the ammonium nitrate solution of the container is renewed.

Before immersion in the ammonium nitrate solution, the specimens had been sandblasted to remove a thin layer of calcite formed on the specimen surface during the storage phase, which might slow down or prevent the degradation of the specimens. The degradation depths are measured at 4 experimental terms for each specimen: 4, 8, 14 and 30 weeks. For each experimental time intervals, the specimens are taken from the containers, and a slice is sawn, on which the degradation depth is revealed with phenolphthalein. The thickness of the slice is adapted to the experimental interval (the longer the specimen has been immersed in ammonium nitrate solution, the larger the slice). The rest of the concrete specimen is then placed back in the ammonium nitrate solution container. Phenolphthalein is a pH indicator through colorimetric reaction: the sound part of the concrete has a highly basic pH so that the phenolphthalein turns pink, whereas the degraded area has a pH below the

colorimetric threshold of the phenolphthalein, and therefore remains grey. Actually, it seems that the degradation depth revealed with phenolphthalein is not exactly the position of the portlandite dissolution front [30], but the ratio between both is not completely acknowledged; this is the reason why in this study for practical reasons the degradation depth is considered to be equal to the one revealed by phenolphthalein. In Figure 17 one can observe the degradation depths revealed with phenolphthalein for the 4 experimental terms on the very same specimen.

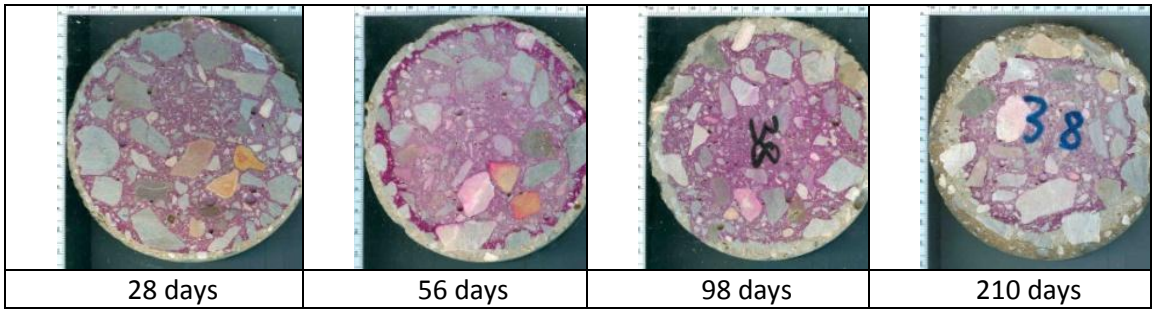

Figure 17 - Degradation depths observed on the same specimen (batch 38 of A1 concrete) at the 4 experimental time intervals of the ammonium nitrate leaching test.

For every experimental test interval, each specimen is scanned to obtain a digital image of the sawn slice of concrete after spraying with phenolphthalein. The degradation depth is then numerically evaluated over about a hundred radiuses. For these measurements, special care has been taken to avoid the influence of aggregates particles: the degradation has been measured on mortar exclusively. The average coefficient of variation of the degradation depth measured on a concrete specimen (about a hundred values) is 13% at 28 days, 12% at 56 days, 10% at 98 days and finally 8% at 210 days. This decreasing coefficient of variation is partly explainable by the fact that the radius of the sound concrete decreases with time, therefore the perimeter for the measurement of the degradation depth decreases as well.

In Table 10, for every concrete mix and each experimental test interval (4, 8, 14 and 30 weeks), a comparison is made between the average degraded depth, the coefficient of variation as well as the number of considered specimens. It can be noted that the degradation seems to be faster for the concrete of the second construction site than for the first one. However, all specimens do not undergo the same temperature history during the leaching test (since the specimens are immersed in the ammonium nitrate solution at rate of 8 specimens every 8 weeks). Therefore, the variability observed on the degradation depths, and presented in Table 11, includes the influence of temperature variations and, thus, is not considered representative of the variability of the material.

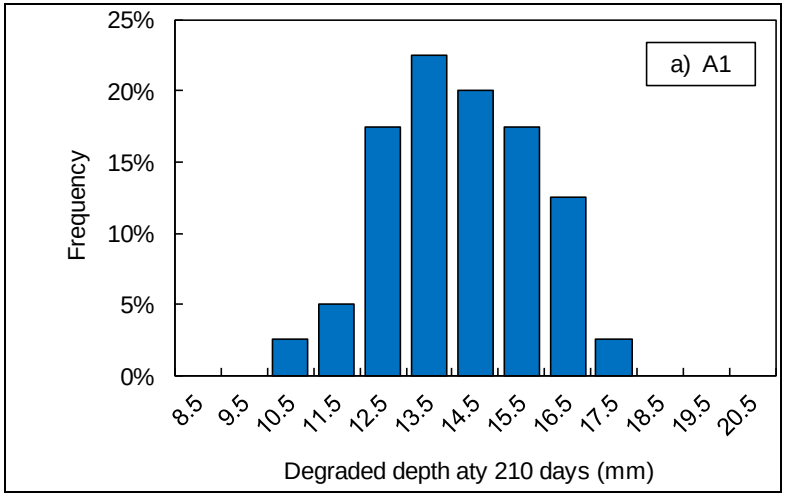

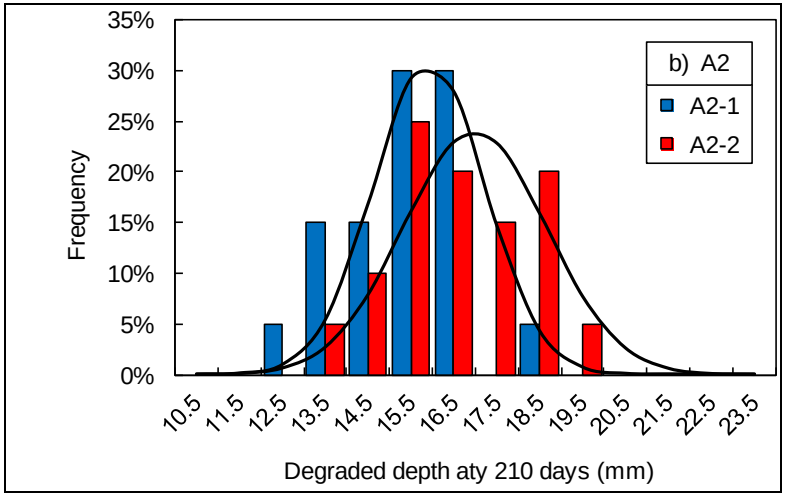

429 Figure 18 – Degraded depth distribution at 96 days (accelerated degradation using ammonium nitrate).

430

431 Table 11 – Degradation depths observed in the accelerated leaching test: number of specimens tested (Nb), mean value and coefficient of
432 variation.

		28 days		56 days		96 days		210 days	
Site	Nb	Mean	COV	Mean	COV	Mean	COV	Mean	COV
A1	40	4.2	20.8%	6.3	19.4%	8.8	16.8%	14.6	10.1%
A2-1	20	4.6	10.9%	7.0	8.1%	9.8	8.0%	15.9	8.1%
A2-2	20	6.0	12.0%	10.2	12.7%	12.8	9.9%	17.0	9.8%

433

434 In order to eliminate the influence of temperature in the interpretation of the accelerated leaching tests, so as to assess the material
435 variability, two modelling approaches have been proposed. The first approach is a global macroscopic modelling based on the hypothesis that
436 the leaching kinetics are proportional to the square root of time and thus that the process is thermo-activated. This means that an Arrhenius law
437 can be applied on the slope of the linear function giving the degradation depth with regard to the square root of time (4). The basic idea of this
438 approach is to determine, from the degradation depths measured at the four experimental intervals for every specimen, one scalar parameter

representative of the kinetics of the degradation but independent from the temperature variations experienced by the specimen during the test. This scalar parameter is denoted k_0 in equation (4) See [27] for more details.

$$e(t,T) = k(T)\sqrt{t} = k_0 \exp\left(-\frac{E_A}{RT}\right)\sqrt{t} \quad (4)$$

The second approach is presented in more detail in de [31]: it is a simplified model for calcium leaching under variable temperature in order to simulate the tests performed within the APPLET project. This approach is based on the mass balance equation for calcium (5) [32, 33], under the assumption of a local instantaneous chemical equilibrium, and combined with thermo-activation laws for the diffusion process and the local equilibrium of calcium. It appears that among the input parameters of this model, the most influential on the leaching kinetics are the porosity ϕ and the coefficient of tortuosity coefficient τ, which is a macroscopic parameter to model the influence of coarse aggregates on the kinetics of diffusion through the porous material [34]. This tortuosity coefficient, although not directly measurable by experiments, is nevertheless identifiable by inverse analysis. The main difference between τ and the parameter k_0 of the global thermo-activation of the leaching process is that τ is by definition independent from both temperature and porosity.

$$\frac{\partial}{\partial t}\left(\phi C_{Ca}\right) = -div\left[-\tau D_0 e^{k\phi} grad\left(C_{Ca}\right)\right] - \frac{\partial S_{Ca}}{\partial t} \quad (5)$$

455 Table 12 summarizes the variability that has been observed for the materials studied within the APPLET program through the accelerated
456 leaching test. In this table one may consider the mean value and coefficient of variation for the material porosity ϕ, the coefficient τ and the
457 parameter of the global thermo-activation of the leaching process k_0. It appears that the tortuosity is significantly lower for the first concrete
458 formulation (site A1) slower degradation kinetics), but for the two formulations of the second site, the coefficient has exactly the same mean
459 value, and only the variability decreases (which was the objective sought by the readjustment of the concrete formulation). This equality
460 between the two formulations of the second construction operation could not be foreseen through the degradation depths (Table 11) or the
461 parameter k_0 (Table 12). This difference in the mean values for k_0 (whereas the mean values for τ are identical) may be interpreted as the
462 influence of the porosity, which is a highly important parameter on the kinetics of degradation, and that this is integrated in parameter k_0 but not
463 in the coefficient of tortuosity coefficient τ.
464

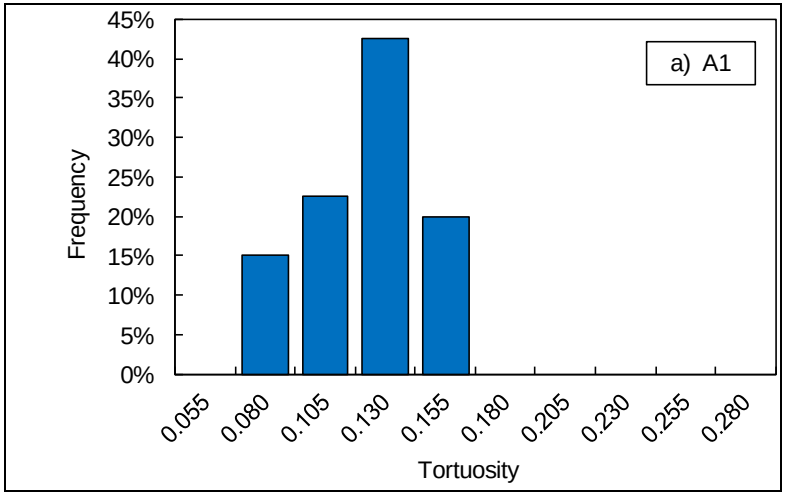

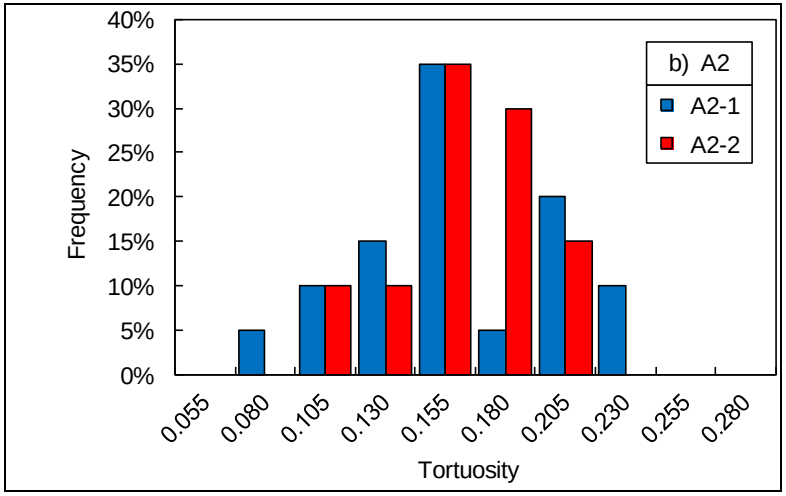

465 Figure 19 – Tortuosity distribution (using ammonium nitrate).

466

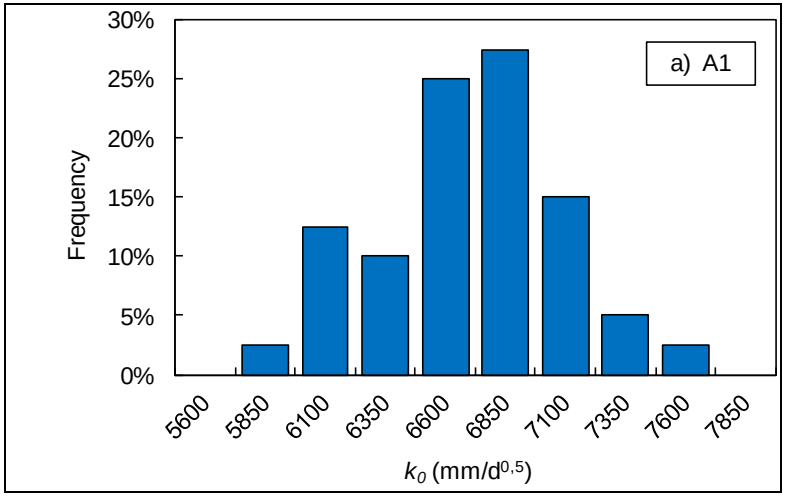

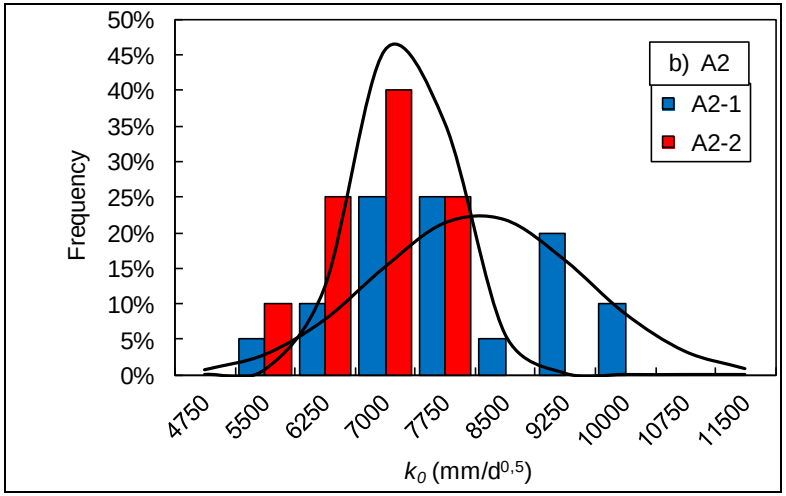

Figure 20 – Accelerated degradation kinetics distribution (using ammonium nitrate). The solid lines are guides for the eyes only (normal probability density function).

Table 12 – Measured and identified variability of the porosity ϕ, the coefficient of tortuosity coefficient τ and the parameter k_0 of global thermo-activation of the leaching process.

		Porosity ϕ		Tortuosity τ		Kinetics k_0 [mm/d$^{0.5}$]	
	Nb	Average	COV	Average	COV	Average	COV
A1	40	12.9%	7.9%	0.134	15.1%	6.82	5.6%
A2-1	20	14.4%	9.0%	0.173	24.5%	8.17	16.2%
A2-2	20	14.1%	4.0%	0.173	17.5%	7.25	8.3%

3.8. Permeability

The gas permeability of the concrete produced at the first construction site (A1 site) was characterized at CEA using a Hassler cell: this is a constant head permeameter which is very similar to the well-known Cembureau device [35]. The specimens to be used with this device are cylindrical with a diameter equal to 40 mm, and their height can range from a few centimeters up to about ten. The device can be used to apply

an inlet pressure up to 5 MPa (50 atm). The gas flow rate is measured after percolation through the specimen using a bubble flow-meter. The percolation of the gas through the specimen is ensured using an impervious thick casing (neoprene) and a containment pressure up to 6 MPa (60 atm). Note that the latter is independent of the inlet pressure. This device has been used at the CEA for more than ten years for gas permeability measurements [36-38].The difference between the Cembureau and Hassler cells was investigated in another program: the two apparatus showed very similar results [39].

The specimens to be tested (Ø40 mm) were obtained by coring the large specimens (Ø113×226 mm) cast at the first construction site (A1). Both ends of each cored specimen (Ø40×226 mm) were sawn off and discarded. The remaining part was then cut to yield three specimens (Ø40×60 mm, cf. Figure 21). A maximal number of nine specimens could be obtained from each Ø113 mm specimen. According to our experience in concrete permeability measurements, these dimensions (Ø40×60 mm) are sufficient to ensure representative and homogeneous results. Note that the large specimens (Ø113×226 mm) were kept under water (with lime at 20°C) for eleven months before use as to ensure optimal hydration and prevent carbonation.

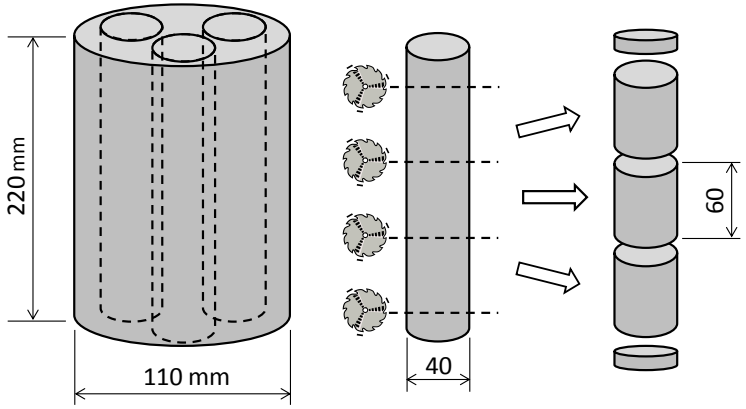

Figure 21 – Preparation of the specimens for the gas permeability measurements.

Before the permeability characterization, the specimens were completely dried at 105°C (that is to say until constant weight) according to the recommendations [25, 35]. This pre-treatment is known to induce degradation of the hardened cement paste hydrates. Yet it appeared as the best compromise between representativeness, drying complexity and duration. From a practical point of view, the complete drying was achieved in less than one month. After the drying, the specimens were let to cool down in an air-conditioned room at 20°C ± 1°C in a desiccator above silica gel (in order to prevent any water ingress).

After this pretreatment the permeability tests were performed using nitrogen (pure at 99.995%) in an air-conditioned room (20°C ± 1°C) in which the specimens were in thermal equilibrium. The measurement of the gas flow rate at the outlet (after percolation through the specimen) and when the steady state was reached (constant flow-rate) allowed the evaluation of the effective permeability K_e [m^2] [40]. The intrinsic permeability was then estimated using the approach proposed by Klinkenberg [40, 41]. The latter allows the estimation of the impact of the gas

slippage phenomenon on the measured effective permeability K_e: in practice the effective permeability K_e is a linear function of the intrinsic permeability K [m^2] and the inverse of the test average pressure $\bar{P}$ [Pa]:

$$K_e = K\left(1 + \frac{\beta}{\bar{P}}\right) \quad (6)$$

where β is the Klinkenberg coefficient [Pa] which accounts for the gas slippage. From a practical point of view at least three injection steps (typically 0.15, 0.30 and 0.60 MPa) were used to estimate the intrinsic permeability K. A unique value of the confinement pressure was used for all the tests: 1.5 MPa. One Ø113 mm specimen per batch was used and the first nine batches collected from the first construction site (A1) were characterized (a total of 75 tests were performed). The results are presented in Figure 21. The open symbols and horizontal error bars stand for the results of each cored specimen and the average value of each batch, respectively.

The concrete intrinsic permeability was found to be ranging between 2.4×10^{-17} and 9.8×10^{-17} m^2 with an average value equal to 5.6×10^{-17} m^2 (by averaging the average values for all the nine batches). This is in good agreement with the results obtained by [37] using the same preconditioning procedure and a similar concrete (CEM I, w/c = 0.43): 6.6×10^{-17} m^2. The standard deviation is equal to 1.2×10^{-17} m^2; which gives a coefficient of variation equal to 22%. This value is of the same order of magnitude than for the other transport properties investigated in this study.

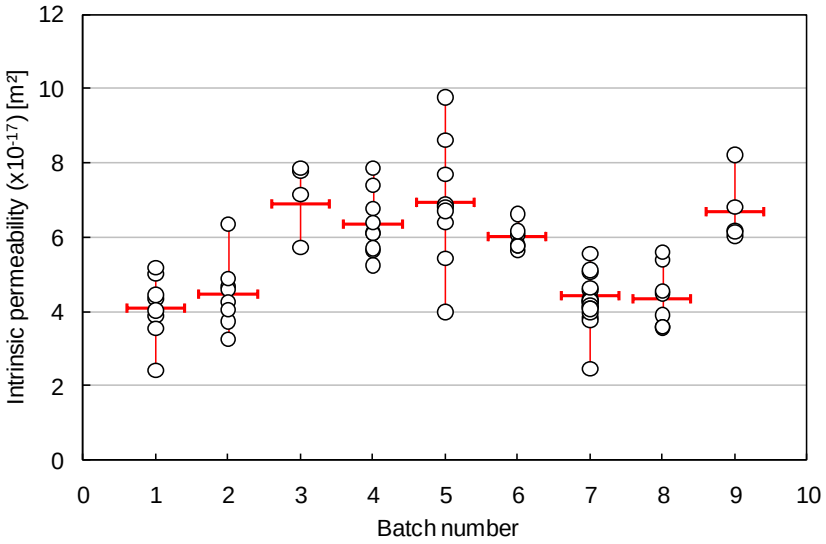

Figure 21 – Intrinsic permeability (using nitrogen) of the first nine batches (construction site A1). Each circle corresponds to an experimental value obtained using a cored specimen. The horizontal bar stands for the mean value for each batch.

The results emphasize the important variability which can be encountered within a Ø113 mm specimen: for instance for batch 5, the permeability was found to vary by a factor of 2. This variability is very unusual with regard to our experience in permeability measurements of laboratory concretes. It is believed that the specimens manufacturing on site by the site workers in industrial conditions (time constraints, large concrete volume to be placed) did result in the decrease of the concrete placement quality compared to laboratory fabrication [42, 43]. This point was supported by the presence of large air voids (about one centimeter large) within the specimens which could be occasionally detected during the coring operations. These voids are also believed to contribute to the permeability increase [44].

527 Note that the intrinsic variability of the test itself was estimated; a permeability test was repeated ten times using the same specimen (after a
528 test the specimen was removed from the permeameter, left in a desiccator for at least one day and then tested again). The measurements
529 standard deviation was equal to 0.17×10^{-17} m^2 (for an average value equal to 4.1×10^{-17} m^2). The coefficient of variation is about 4%, which is far
530 less than the variability observed. For clarity, in figure 21 the uncertainty related to the test corresponds to the symbol height.
531 Simultaneously, experiments were conducted at LML: permeability was measured using cylindrical specimens (diameter: 37 mm – height:
532 about 74 mm) cored from bigger moulded specimens of the A1 construction site (batch A1-13). The specimens, until testing, were always kept
533 immersed in lime saturated water at 20 ± 2°C. Permeability was measured by gas (argon) percolation in a triaxial cell on small specimens dried in
534 oven at 90°C or at 90 then at 105°C until mass equilibrium. The choice of argon as a percolating gas is due to its inert behavior with cement,
535 allowing an adequate measure of the material permeability. The whole experimental permeability measurement device is composed of a triaxial
536 cell that allows the application of a confining pressure on the specimen through oil injection. The specimen is equipped with a drainage disc
537 (stainless steel with holes and lines ensuring a one-dimensional homogenous gas flow at the surface of the specimen) at each end. The specimen
538 is then placed in the bottom section of the cell where the gas pressure Pi will be applied. A drainage head, to allow flowing of gas to the exterior
539 of the cell (atmospheric pressure Pf) after the percolation through the specimen, is placed on the upper part of the specimen. Then a protective
540 jacket is put around the specimen and the drainage devices to isolate the specimen where gas flows from confining oil ingress. A sketch of this
541 permeability cell is presented in Figure 22.
542

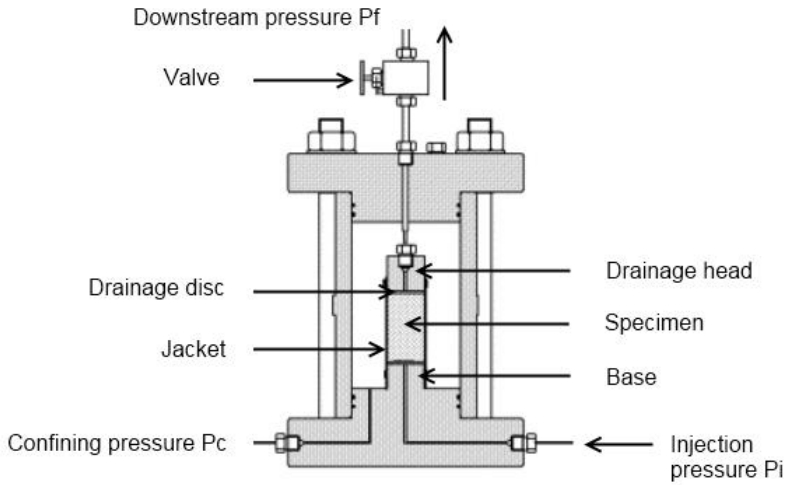

Figure 22 - Sketch of the triaxial cell for permeability measurements at LML.

The measurement procedure and determination of permeability is performed as follows. Once the specimen is in the triaxial cell, confining pressure is increased and kept constant to 4 MPa. Then, the gas is injected at a pressure of about 2 MPa, and the downstream pressure P_f is in equilibrium with atmospheric pressure (0 MPa in relative pressure). This injection is directly done by the reducing valve of the gas bottle, which also feeds a buffer circuit. This phase is pursued until a permanent gas flow inside the specimen is achieved. This is detected by a stabilization of the injection pressure P_i. At this moment, the reducing valve is closed, and only the buffer circuit provides gas to the specimen. As a consequence, a drop of pressure appears since gas continues to flow through the specimen. The permeability is deduced from the time Δt needed to get a given change ΔP of the injection pressure. This decrease of injection pressure should remain low to ensure the quasi-permanent flow hypothesis. The volume of the buffer circuit V is known by preliminary tests, and with the perfect gas hypothesis, the effective permeability K_e is calculated using:

555

556 $$K_e = 2\frac{\mu_g Q_m L P_m}{S\left(P_m^2 - P_f^2\right)} \quad (6)$$

557

558 where μ_g is the gas viscosity, L the height of the specimen, S its cross section and P_m the medium pressure given by:

559

560 $$P_m = P_i - \frac{\Delta P}{2} \quad (6)$$

561

562 Q_m is the medium flow, which under isothermal conditions is:

563

564 $$Q_m = \frac{V\Delta P}{P_m \Delta t} \quad (6)$$

565

566 The measured permeability K_e is an effective permeability (and not an intrinsic) being dependent on injection pressure due to the Klinkenberg
567 effect. However, for an injection pressure of 2 MPa, this effect is negligible, as confirmed by additional tests. A refined description of
568 permeability devices can be found in [45] . For our tests, ΔP is 0.025 MPa, the injection pressure varies around 2 MPa (between 2.02 and 2.24
569 MPa). The permeability is determined on 6 specimens from batch A1-13, dried at 90°C, and values are presented in Table 13. The permeability of
570 each specimen is measured two times to evaluate the immediate repeatability (between two measurements, the specimen remains in the cell

under confining pressure, the reducing valve is opened until a permanent gas flow inside the specimen is achieved and finally the second measure is performed). 3 additional specimens from the same batch are firstly dried at 90°C until mass equilibrium, then at 105°C, and their permeability is determined. Table 14 gives an overview of the statistical data of these specimens. The statistical dispersion, as for porosity, has the same order of magnitude at both 90 and 105°C (around 11-12%), and thus the effect of temperature on variability remains negligible.

Table 13 – Permeability after drying at 90°C (batch A1-13).

Specimen	Permeability ($\times 10^{-17}$ m^2)	
	1st run	2nd run
19-3	2.83	2.81
19-5	2.97	2.99
38-2	2.62	2.61
38-3	2.25	-
38-4	2.91	2.88
38-5	3.24	3.24

Table 14 – Statistical data on permeability for dried specimens at 90°C or at 90 and then 105°C (batch A1-13).

	Specimen number	Average permeability ($\times 10^{-17}$ m^2)	Standard deviation ($\times 10^{-17}$ m^2)	Coefficient of variation
90°C	6	2.80	0.34	12.1%
105°C	3	4.40	0.49	11.1%

4. Analysis/discussion

4.1. Construction sites comparison

Table 15 summarizes all the coefficients of variation obtained for all the experiments concerning the two construction sites. The change of mix design during the production at site A2 could be seen on several physical parameters, however not on the mechanical ones. If the entire production of site A2 is considered, except for the chloride migration, the coefficients of variation are very similar between sites A1 and A2. For the chloride migration, there may be an effect of slag on this specific phenomenon.

Table 15 – Coefficients of variation of all the tests.

Test	Laboratory	A1	A2/1	A2/2	A2
Compressive strength	Vinci	7.3%	11.1%	11.1%	12%
Compressive strength	LMT	10.5%	11.3%	11.1%	12%
Tensile strength	LMT	13.3%	9.7%	9.3%	9.9%
Young modulus	LMT	6.2%	8.2%	5.4%	7%
Chloride migration	LMDC	12.4%	25.4%	19.4%	21.9%
Water content at RH=53.5%	LaSIE	14%	7%	Not available	Not available
Carbonation depth	CERIB and LaSIE	37%	35%	12%	33%
Resistivity	I2M	17.9%	15.6%	17.2%	18.5%
Porosity	LMT	7.9%	9%	4%	7%
Degraded depth after 210 days of leaching	LMT	10.1%	8.1%	9.8%	9.5%
Permeability	CEA	22%	Not available	Not available	Not available

590 ## 4.2. Probability density fitting

591 In order to perform lifetime simulations related to durability on the basis of reliability approach, it is necessary to characterize the variability
592 of the model parameters by their appropriate probability density function according to the observed statistical distribution. These density
593 functions can be used as initial or prior estimates for the studies where no data are available. They could be updated, for example using Bayesian
594 techniques, when field data will be available by monitoring or specific investigation of a structure.

595 To determine the most appropriate probability density function that best represent the statistical distribution of the experimental data, an
596 approach by the maximum likelihood estimator (MLE) was used by Oxand [46, 47] . This technique helps to determine among the various
597 probability functions tested the one that has the most important likelihood, *i.e.* the one that is best able to represent the distribution of
598 observations. The suitability of the experimental distribution to the chosen function has not been achieved through an adequacy test
599 (Kolmogorov-Smirnov non-parametric test for the equality of continuous, one-dimensional probability distributions for example) but by simple
600 visual verification considering the small amount of data sometimes available.

601 A fairly wide range of probability density functions has been tested (12 probability density functions, see appendix) to test their adequacy
602 with respect to the MLE principle even if generally, some of them are rarely used to describe physical parameters in civil engineering. The various
603 parameters studied during the experimental campaign were sometimes obtained by different tests and techniques (e.g. the compressive
604 strength of concrete was determined by the experimental device of the contractor and in different research laboratories; permeability was
605 determined using two different procedures). Table 16 summarizes the different probability functions tested and those that are proposed to
606 represent the intrinsic and measurement variability of the different parameters studied during the experimental campaign.

607

608 Table 16 – Summary of the adequacy of the probability density functions tested.

Durability indicator/test	Proposed distribution laws	Other distribution available
Compressive strength	Lognormal, Normal, Extreme	Birnbaum-Sanders, Weibull, Gamma, Rice
Permeability	Lognormal, Gamma	Normal, Weibull, Log-logistique, Nakagami
Resistivity	Lognormal, Gamma	Normal, Weibull, Log-logistic, Nakagami
Density	Extreme, Weibull	Logistic, Log-logistic
Porosity	Lognormal, Gamma	Birnbaum-Sanders, Log-logistic
Leaching	Normal, Lognormal	Birnbaum-Sanders, Extreme, Weibull, Rice
Tensile strength	Lognormal, Gamma	Birnbaum-Sanders, Weibull, Rice, Nakagami
Young's modulus	Lognormal, Gamma	Birnbaum-Sanders, Logistic, Log-logistic
Carbonation depth	Weibull, Normal	Rice
Chloride migration coefficient	Lognormal	Birnbaum-Sanders, Gamma
Poisson’s coefficient	Lognormal, Gamma	Birnbaum-Sanders

609

610 The adequacy procedure based on the maximum likelihood estimator was applied to samples of varying size. The results were interpreted
611 taking into account a rather small number of data for a precise statistical study (depending on the parameter studied, the data processed varied
612 generally between 20 and 40). This may explain the fact that for many parameters, several probability functions seem relatively close without
613 being able to have clear preference for one or the other. For some parameters, due to a very small number of tests carried out, all the available
614 data has been used to fit the statistical distribution even if some of them came from different specimens (this was done for the chloride
615 migration coefficient D_{nssm} for example, see Figure 24).

616 From a practical point of view, and from the perspective of using these results in the context of reliability analysis for the engineer, it may be
617 wise to use "classical" probability functions with parameters that are easy to estimate rather than others that are more difficult to simulate. In
618 this sense, the lognormal distribution has often appeared as one of the most appropriate, together with the gamma, extreme and normal

619 distributions. Figure 23 to Figure 24 illustrate a comparison between experimental and theoretical probability densities and distribution functions

620 for various parameters.

621

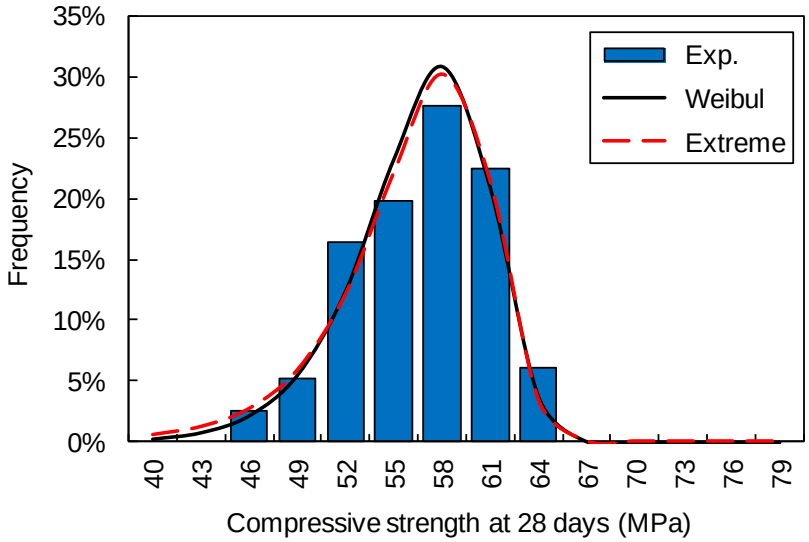

622

623 Figure 23 – Experimental (cf. Figure 4) and theoretical probability densities and distribution functions for the compressive strength of A1

624 concrete at 28 days (sample size: 116).

625

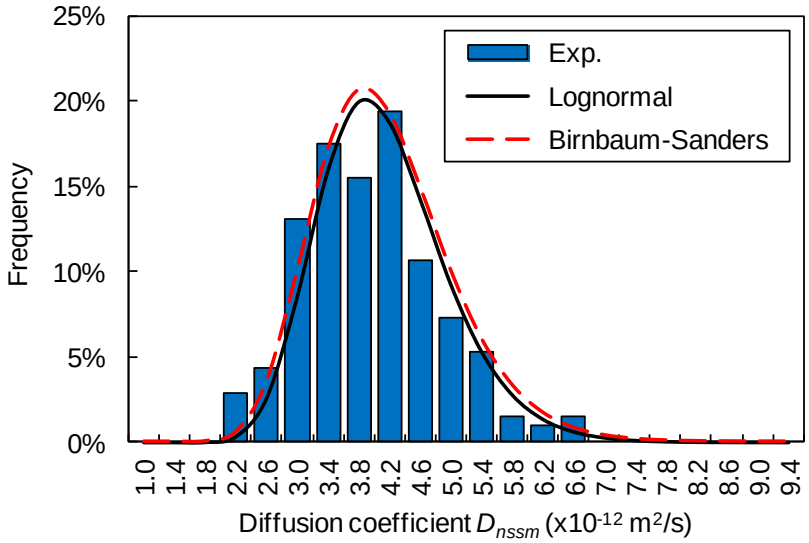

Figure 24 – Probability density and distribution functions for the experimental and theoretical chloride migration coefficient in A1 concrete (sample size: 206).

5. Conclusion

One of the main objectives of the APPLET project (work group 1) was to characterize concretes variability for the assessment of reinforced concrete structures durability. In practice, a quantitative insight of concretes variability was obtained through durability tests and indicators. Forty sets of concrete specimens were taken from two different construction sites over a period of one year and sent to the different project partners to have different characterization tests performed. The specimens were prepared on the two construction sites by the site workers: the authors then believed that the results obtained were representative of the variability of the two concrete formulations prepared in industrial

conditions. Nevertheless, the reader must keep in mind that the variability of the concrete formulations might not fully representative of the variability that can be expected for the structural elements concrete: the latter might be higher.

The results obtained do however constitute a unique dataset of reliable and consistent experimental data that can be used to estimate the variability of concrete properties within existing structures. Fitting using suitable probability density functions allows these data to be used as inputs for probabilistic approaches. From a practical point of view, one could select from the database the parameters that are relevant for his study in terms of physics and chemistry but also sensitivity: depending on the considered phenomena and the associated modeling some parameters with low variability may have a pronounced influence on the outcome and *vice versa*. For example, in the approach of Muigai et al. [48] describing reinforcement chloride-induced corrosion, one should select the chloride migration coefficient as the relevant parameter.

Acknowledgements

The investigations and results reported herein are supported by the National Research Agency (France) under the APPLET research program (grant ANR-06-RGCU-001-01). The authors would like to thank an anonymous reviewer who was very helpful to improve this article.

6. References

[1] C. Cremona, L. Adélaide, Y. Berthaud, V. Bouteiller, V. L'Hostis, S. Poyet, J-M. Torrenti, Probabilistic and predictive performance-based approach for assessing reinforced concrete structures lifetime: the applet project, EPJ Web of Conf. 12 (2011) 01004 (2011).

[2] J-M. Torrenti, P. Dantec, C. BoulayJ-F. Semblat, Projet du processus d'essai pour la détermination du module de déformation longitudinale du béton (in French), Bull. Lab. Ponts Chaussées 220 (1999) 79-81.
[3] S.A. Mirza, M. Hatzinikolas, J.G. McGregor, Statistical descriptions of strength of concrete, ASCE J. Struct. Div. 105 (1979) 1021-1037.
[4] T. Chmielewski, E. Konopka, Statistical evaluations of field concrete strength." Mag. Concr. Res. 51 (1999) 45-52.
[5] J-M. Torrenti, Vers une approche probabiliste de la durabilité : application au cas de stockage de déchets nucléaires (in French), In : Conference GC'2005, Paris, France, 2005.
[6] F. Cussigh, V. Bonnard, C. Carde, O. Houdusse, Rion-Antirion bridge project – concrete durability for prevention of corrosion risks, in: Toutlemonde *et al.* (Eds.), proceedings of the International Conference on Concrete Under Severe Conditions (CONSEC'07), Tours, France, 2007, pp. 839-850.
[7] NT Build 492, Concrete, mortar and cement-based repair materials: chloride migration coefficient from non-steady-state migration experiments, Nordtest method, 1999, 8p.
[8] F. Deby, M. Carcassès, A. Sellier, Simplified models for the engineering of concrete formulations in a marine environment through a probabilistic method, Eur. J. Env. Civ. Eng. 16 (2012) 362-374.
[9] F. Deby, M. Carcassès, A. Sellier, Probabilistic approach for durability design of reinforced concrete in marine environment, Cem. Concr. Res. 39 (2009) 466-471.
[10] A. Trabelsi, A. Hamami, R. Belarbi, P. Turcry, A. Aït-Mokhtar, Assessment of the variability of moisture transfer properties of High Performance Concrete from multi-stages drying experiment, Eur. J. Env. Civ. Eng. 16 (2012) 352-361.
[11] R. Belarbi, A. Aït-Mokhtar, M. Qin, O. Omikrine, Development of simplified approach to model the moisture transfer of building materials, Eur. J. Env. Civ. Eng. 10 (2006) 1033-1048.
[12] V. Baroghel-Bouny, Water vapour sorption experiments on hardened cementitious materials. Part II: Essential tool for assessment of transport properties and for durability prediction, Cem. Concr. Res. 37 (2007) 438-454.
[13] K.S.W. Sing, D.H. Everett, R.A.W. Haul, L. Moscou, R.A. Pierotti, J. Rouquérol, T. Siemieniewska, Reporting physisorption data for gas/solid systems, Pure Appl. Chem. 57 (1985) 603-619.
[14] A. Trabelsi, R. Belarbi, P. Turcry, A. Aït-Mokhtar, Water vapour desorption variability of in situ concrete and effects on drying simulations, Mag. Concr. Res. 63 (2011) 333-342.
[15] P. Turcry, A. Younsi, F. Jacquemot, A. Aït-Mokhtar, P. Rougeau, Influence of in situ concrete variability on accelerated carbonation test, Eur. J. Env. Civ. Eng. 16 (2012) 288-297.
[16] G.G. Litvan, A. Meyer, Carbonation of Granulated Blast Furnace Slag cement concrete during twenty years of field exposures, in: Malhotra (Ed.) proceedings of the 5th international conference on fly ash, silica fume, slag and natural pozzolans in concrete, Madrid, Spain, 1986, ACI SP-91, pp. 1445-1462.
[17] M. Maage, Carbonation in concrete made of blended cements, Mater. Res. Symp. Proc. 65 (1986) 193-198.
[18] C. Andrade, C. Alsonso, A. Arteaga, P. Tanner, Methodology based on the electrical resistivity for calculation of reinforcement service life, in: Malhotra (Ed.) proceedings of the 5th CANMET/ACI International Conference on Durability of Concrete, Barcelona, Spain, 2000, pp. 899-915.
[19] E.J. Garboczi, Permeability, diffusivity and microstructural parameters: a critical review, Cem. Concr. Res. 20 (1990) 591-601.

687 [20] O. Francy, Modélisation de la pénétration des ions chlorures dans les mortiers partiellement saturés en eau (in French), Ph.D. thesis, Paul
688 Sabatier university, Toulouse, France, 1998, 171p.
689 [21] F. Rajabipour, W.J. Weiss, D.M. Abraham, Insitu electrical conductivity measurements to assess moisture and ionic transport in concrete (a
690 discussion of critical features that influence the measurements), in: Weiss et al. (Eds) proceedings of the 1st international RILEM
691 symposium on Advances in Concrete through Science and Engineering, March 21-26, 2004, Evanston, 18p.
692 [22] V. Baroghel-Bouny, Conception des bétons pour une durée de vie donnée des ouvrages – indicateur de durabilité (in French), Document
693 Scientifique et Technique AFGC, 2004, 252p.
694 [23] J-F. Lataste, T. de Larrard, F. Benboudjema, J. Séménadisse, Electrical resistivity variability of two concretes: protocol study in laboratory
695 and assessment on site, Eur. J. Env. Civ. Eng. 16 (2012) 298-310.
696 [24] I.L.H. Hansson, C.M. Hansson, Electrical resistivity measurements of Portland cement-based materials, Cem. Concr. Res. 13 (1983) 675-683.
697 [25] AFPC-AFREM, Durabilité des bétons – Méthodes recommandées pour la mesure des grandeurs relatives à la durabilité (in French),
698 proceedings of the technical meeting AFPC-AFREM, december 1997, Toulouse, France, 1997.
699 [26] F. Zhang, T. Rougelot, N. Burlion, Porosity of concrete: Influence of test conditions and material variability, Eur. J. Env. Civ. Eng. 16 (2012)
700 311-321.
701 [27] T. de Larrard, S. Poyet, M. Pierre, F. Benboudjema, P. Le Bescop, J-B. Colliat, J-M. Torrenti, Modelling the influence of temperature on
702 accelerated leaching in ammonium nitrate, Eur. J. Env. Civ. Eng. 16 (2012) 322-335.
703 [28] S. Poyet, P. Le Bescop, M. Pierre, L. Chomat, C. Blanc, Accelerated leaching using ammonium nitrate (6M): influence of test conditions, Eur.
704 J. Env. Civ. Eng. 16 (2012) 336-351.
705 [29] F.M. Lea, The action of ammonium salts on concrete, Mag. Concr. Res. 17 (1965) 115-116.
706 [30] C. Le Bellego, Couplage chimie-mécanique dans les structures en béton attaquées par l'eau: étude expérimentale et analyse numérique (in
707 French), Ph.D. thesis, Ecole Normale Supérieure de Cachan, France, 2001, 236p.
708 [31] T. de Larrard, F. Benboudjema, J-B. Colliat, J-M. Torrenti, F. Deleruyelle, Concrete calcium leaching at variable temperature: experimental
709 data and numerical model inverse identification, Comput. Mater. Sci. 49 (2010) 35-45.
710 [32] M. Buil, E. Revertégat, J. Oliver, A model for the attack of pure water or undersaturated lime solutions on cement, In: Gilliam & Wiles (Eds.)
711 Stabilization and Solidification of Hazardous Radioactive and Mixed Wastes, ASTM STP 1123 1992, pp. 227-241.
712 [33] M. Mainguy, C. Tognazzi, J-M. Torrenti, F. Adenot, Modelling of leaching in pure cement paste and mortar, Cem. Concr. Res. 30 (2000) 83-
713 91.
714 [34] V.H. Nguyen, B. Nedjar, H. Colina, J-M. Torrenti, A separation of scales homogenisation analysis for the modelling of calcium leaching in
715 concrete, Comput. Methods Appl. Mech. Eng. 195 (2006) 7196-7210.
716 [35] J.J. Kollek, The determination of the permeability of concrete to oxygen by the Cembureau method – a recommendation, Mater. Struct. 22
717 (1989) 225-230.
718 [36] C. Gallé, J-F. Daïan, Gas permeability of unsaturated cement-based materials: application of a multi-scale network model, Mag. Concr. Res.
719 52 (2000) 251-263.
720 [37] C. Gallé, J. Sercombe, Permeability and pore-structure evolution for silico-calcareous and hematite high-strength concretes submitted to
721 high temperatures, Mater. Struct. 34 (2001) 619-628.

[38] M.C.R. Farage, J. Sercombe, C. Gallé, Rehydration and microstructure of cement paste after heating at temperatures up to 300°C, Cem. Concr. Res. 33 (2003), 1047-1056.
[39] P. Kalifa, G. Chéné, C. Gallé, High-temperature behaviour of HPC with polypropylene fibres: from spalling to microstructure, Cem. Concr. Res. 31 (2000) 1487-1499.
[40] P.A.M. Basheer, Permeation analysis, In: Ramachandran & Beaudouin (Eds), Handbook of analytical techniques in concrete science and technology, Noyes Publications, Park Ridge, New Jersey, USA, 2001, pp. 658-737.
[41] L.J. Klinkenberg, The permeability of porous media to liquid and gases, Drill. Prod. Pract. Am. Pet. Inst. (1941) 200-214.
[42] A.M. Vaysburd, C.D. Brown, B. Bissonnette, P.H. Emmons, Realcrete versus Labcrete, Concr. Int. 26 (2004) 90-94.
[43] S. Poyet, X. Bourbon, Experimental investigation of concrete packages for radioactive waste management: permeability and influence of junctions, Transp. Porous Med. 95 (2012) 55-70.
[44] H.S. Wong, A.M. Pappas, R.W. Zimmerman, N.R. Buenfeld, Effect of entrapped air voids on the microstructure and mass transport properties of concrete, Cem. Concr. Res. 41 (2011) 1067-1077.
[45] H. Loosveldt, Z. Lafhaj, F. Skoczylas, Experimental study of gas and liquid permeability of a mortar, Cem. Concr. Res. 32 (2002) 1357-1363.
[46] R.A. Fisher, On the mathematical foundations of theoretical statistics, Philosoph. T. Roy. Soc. A 222 (1922) 309-368.
[47] A.W.F. Edwards, Likelihood, Cambridge University Press, 1972, 243p.
[48) R. Muigai, P. Moyo, M. Alexander, Durability design of reinforced concrete structures: a comparison of the use of durability indexes in the deemed-to-satisfy approach and the full-probabilistic approach, Mater. Struct. 45 (2012) 1233-1244.

7. Appendix: probability density functions

Name	Density function	Parameters
Birnbaum-Sanders	$f(x)=\frac{1}{\gamma\beta\sqrt{8\pi}}\left[\left(\frac{\beta}{x}\right)^{\frac{1}{2}}+\left(\frac{\beta}{x}\right)^{\frac{3}{2}}\right]exp\left[-\frac{1}{2\gamma^2}\left(\frac{x}{\beta}+\frac{\beta}{x}-2\right)\right]$	$x>0 \quad \gamma,\beta>0$ Mean value = $\left(1+\frac{\gamma^2}{2}\right)\beta$ Standard deviation = $\gamma\beta\sqrt{1+\frac{5}{4}\gamma^2}$
Exponential	$f(x)=\lambda exp(-\lambda x)$	$x\geq 0$ Mean value = λ^{-1} Standard deviation = λ^{-1}

Extreme	$f(x)=\frac{1}{\sigma}exp\left(\frac{x-\mu}{\sigma}\right)exp\left[-exp\left(\frac{x-\mu}{\sigma}\right)\right]$	Mean value = $\mu+\gamma\sigma$ (where γ is the Euler-Mascheroni constant ≈ 0.577) Standard deviation = $\frac{\pi}{\sqrt{6}}\sigma$
Gamma	$f(x)=x^{k-1}\frac{exp\left(-\frac{x}{\vartheta}\right)}{\Gamma(k)\vartheta^{k}}$	$x\geq 0 \quad k,\vartheta>0$ Γ is the gamma function Mean value = $k\vartheta$ Standard deviation = $\sqrt{k\vartheta}$
Log-logistic	$f(x)=\frac{\beta}{\alpha}\left(\frac{x}{\alpha}\right)^{\beta-1}\left[1+\left(\frac{x}{\alpha}\right)^{\beta}\right]^{-2}$	$x\geq 0 \quad \alpha,\beta>0$ Mean value = $\frac{\pi\alpha}{\beta sin\left(\frac{\pi}{\beta}\right)}$ Standard deviation = $\alpha\sqrt{\frac{2\pi}{\beta sin\left(\frac{2\pi}{\beta}\right)}-\frac{\pi^2}{\beta^2 sin\left(\frac{\pi}{\beta}\right)}}$
Logistic	$f(x)=\frac{1}{s}exp\left(-\frac{x-\mu}{s}\right)\left[1+exp\left(-\frac{x-\mu}{s}\right)\right]^{-2}$	$s>0$ Mean value = μ Standard deviation = $\frac{\pi s}{\sqrt{3}}$
Lognormal	$f(x)=\frac{1}{x\sigma\sqrt{2\pi}}exp\left[-\frac{(ln(x)-\mu)^2}{2\sigma^2}\right]$	$x\geq 0$ Mean value = $exp\left[\frac{1}{2}\left(\mu+\sigma^2\right)\right]$ Standard deviation = $exp\left(\mu+\frac{\sigma^2}{2}\right)\sqrt{exp\left(\sigma^2\right)-1}$
Nakagami	$f(x)=\frac{2\mu^{\mu}}{\Gamma(\mu)\omega^{\mu}}x^{2\mu-1}exp\left(-\frac{\mu}{\omega}x^2\right)$	$x>0 \quad \mu\geq 0.5 \quad \omega>0$ Mean value = $\frac{\Gamma(\mu+0.5)}{\Gamma(\mu)}\sqrt{\frac{\omega}{\mu}}$ Γ is the gamma function

		Standard deviation = $\sqrt{\omega}\sqrt{1-\frac{1}{\mu}\left[\frac{\Gamma(\mu+0.5)}{\Gamma(\mu)}\right]^2}$
Normal	$f(x)=\frac{1}{\sigma\sqrt{2\pi}}exp\left[-\frac{(x-\mu)^2}{2\sigma^2}\right]$	Mean value = μ Standard deviation = σ
Rayleigh	$f(x)=\frac{x}{\sigma^2}exp\left(-\frac{x^2}{2\sigma^2}\right)$	$x>0 \quad \sigma>0$ Mean value = $\sigma\sqrt{\frac{\pi}{2}}$ Standard deviation = $\sigma\sqrt{2-\frac{\pi}{2}}$
Rice	$f(x)=\frac{x}{\sigma^2}I_0\left(\frac{\upsilon x}{\sigma}\right)exp\left(-\frac{x^2+\upsilon^2}{2\sigma^2}\right)$	$x\geq 0 \quad \sigma,\upsilon>0$ I_0 is the Bessel function of order 0 Mean value = $\sigma\sqrt{\frac{\pi}{2}}L_{0.5}\left(-\frac{\upsilon^2}{2\sigma^2}\right)$ L_n is the n^{th} Laguerre's polynomial Standard deviation = $\sqrt{2\sigma^2+\upsilon^2-\sigma^2\frac{\pi}{2}L_{0.5}^2\left(-\frac{\upsilon^2}{2\sigma^2}\right)}$
Weibul	$f(x)=\frac{k}{\lambda}\left(\frac{x}{\lambda}\right)^{k-1}exp\left[-\left(\frac{x}{\lambda}\right)^k\right]$	$x\geq 0 \quad \lambda,k>0$ Mean value = $\lambda\Gamma\left(1+\frac{1}{k}\right)$ Γ is the gamma function Standard deviation = $\sqrt{\lambda^2\Gamma\left(1+\frac{2}{k}\right)-\lambda^2\Gamma^2\left(1+\frac{1}{k}\right)}$

742
743